
MIRA: Medical Time Series Foundation Model for Real-World Health Data

Hao Li^{1,2} [♦] Bowen Deng³ Chang Xu¹ [♣] Zhiyuan Feng⁴
Viktor Schlegel^{2,5} Yu-Hao Huang⁶ Yizheng Sun² Jingyuan Sun²
Kailai Yang² Yiyao Yu⁴ Jiang Bian¹

¹ Microsoft Research ² University of Manchester ³ Peking University
⁴ Tsinghua University ⁵ Imperial College London ⁶ Nanjing University

Abstract

A unified foundation model for medical time series—pretrained on open access and ethics board-approved medical corpora—offers the potential to reduce annotation burdens, minimize model customization, and enable robust transfer across clinical institutions, modalities, and tasks, particularly in data-scarce or privacy-constrained environments. However, existing generalist time series foundation models struggle to handle medical time series data due to their inherent challenges, including irregular intervals, heterogeneous sampling rates, and frequent missing values. To address these challenges, we introduce **MIRA**, a unified foundation model specifically designed for medical time series forecasting. MIRA incorporates a *Continuous-Time Rotary Positional Encoding* that enables fine-grained modeling of variable time intervals, a *frequency-specific mixture-of-experts layer* that routes computation across latent frequency regimes to further promote temporal specialization, and a *Continuous Dynamics Extrapolation Block* based on Neural ODE that models the continuous trajectory of latent states, enabling accurate forecasting at arbitrary target timestamps. Pretrained on a large-scale and diverse medical corpus comprising over 454 billion time points collect from publicly available datasets, MIRA achieves reductions in forecasting errors by an average of 10% and 7% in out-of-distribution and in-distribution scenarios, respectively, when compared to other zero-shot and fine-tuned baselines. We also introduce a comprehensive benchmark spanning multiple downstream clinical tasks, establishing a foundation for future research in medical time series modeling.

1 Introduction

Medical time series data, including signals such as electrocardiograms (ECG) [1], electroencephalograms (EEG) [2], vital signs and laboratory measurements [3], are key to understanding the dynamic physiological states of patients over time [4, 5]. Continuously modeling these patient data trajectories supports clinical forecasting tasks such as predicting organ failure or treatment response [1, 6], enabling earlier decisions and better patient outcomes [7, 8]. However, effectively utilizing medical time series data in practice remains challenging, as patient populations, disease profiles, and clinical protocols can vary widely across regions and institutions. Moreover, such data is often collected in an irregular and asynchronous manner [9, 10], further complicating efforts to build generalizable models. These challenges are compounded by regulatory constraints such as GDPR [11, 12], which inhibit data sharing and result in institutions training task-specific models from scratch on local data,

[♦] Work done during research internship at Microsoft Research.

[♣] Corresponding author: chanx@microsoft.com.

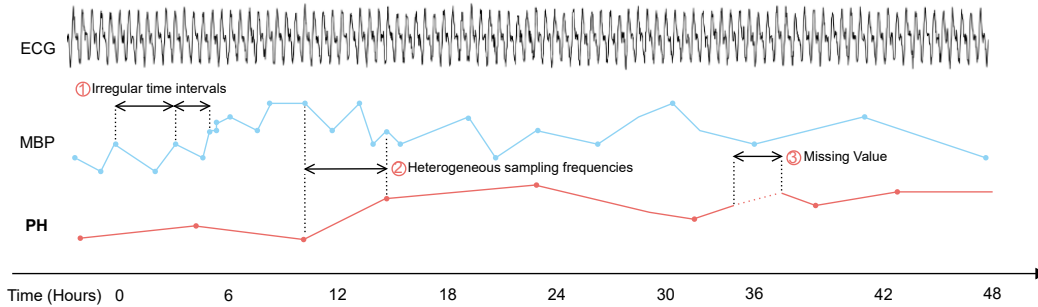


Figure 1: Medical time series exhibit ① irregular intervals, ② heterogeneous sampling rates, and ③ frequent missingness driven by clinical workflows.

incurring significant resource overhead. This highlights the need for a shareable medical foundation model trained on validated, open medical time series datasets, that is able to learn generalizable patterns from large and varied datasets, reducing the need for extensive data annotation and custom model building, while also helping to share knowledge effectively across different clinical institutions, data types, and medical tasks [13, 14].

However, creating effective medical foundation models for time series is challenging, because clinical data are inherently highly irregular and varied: signals like ECGs recorded at millisecond intervals [15] are found alongside laboratory tests conducted hours apart [16] (Figure 1). Differences in clinical workflows and equipment limits result in irregular sampling, missing values, and inconsistent temporal dependencies [17, 18]. Furthermore, physiological variables differ widely in their value and frequency ranges, requiring models that can handle these varied scales and types of data. Traditional methods using medical task-specific time-series models [19–24], trained on isolated datasets, often do not generalize well to new situations and are difficult to scale [25, 26, 9]. Meanwhile recent general-purpose time series foundation models [27–32] show promise, but they usually assume uniform time intervals. Similarly, emerging medical time series foundation models demonstrate cross-dataset generalization but only within narrowly defined domains—for example, across EEG datasets for sleep monitoring or across datasets for Alzheimer’s diagnosis, and cannot handle continuous-time forecasting or irregular sampling [33–36]. These gaps—where current models struggle with the complex, irregular, and multi-frequency nature of medical data [27, 37]—motivates our research and raises a central question:

How can we design a scalable and generalizable foundation model that captures the irregularity and multi-frequency nature of medical time series, while enabling robust transfer across diverse medical tasks?

To address this central question, we introduce **MIRA**—a **MEDICAL FOUNDATION MODEL FOR IRREGULARITY ADAPTATION**. MIRA is specifically designed to address the challenges of medical time series: First, we propose a *Continuous-Time Rotary Positional Encoding (CT-RoPE)*, which extends the standard RoPE [38] to handle time values using learnable frequency adjustments, allowing MIRA to accurately model the varying frequency intervals of irregularly sampled data. Second, to further improve its ability to adapt to different time features in medical signals, MIRA uses a frequency-specific mixture-of-experts (MoE) layer that learns to route frequency-related information through specialized components. Finally, MIRA integrates a Continuous Dynamics Extrapolation Block, using Neural Ordinary Differential Equations (Neural ODEs) [39]. This feature allows the model to predict patient health paths at any future time point, moving beyond the limits of fixed observation grids. MIRA is pretrained on a large curated collection of medical time series, comprised of over 454 billion time points from publicly available datasets. These datasets cover readings from intensive care units (ICUs), operating rooms, pediatric critical care, and long-term sleep and mental health monitoring. All data undergo preprocessing that standardizes time alignment, normalizes sampling frequencies, and maintains clinical realism. MIRA outperforms other time series foundation models with a similar number of parameters across various real-world benchmarks, achieving reductions in forecasting errors by an average of 10% and 7% in out-of-distribution and in-distribution scenarios, respectively.

To summarize, this paper makes the following contributions: **First**, we propose **MIRA**, a new foundation model specially designed for medical time series forecasting. MIRA directly tackles the challenges of irregular sampling and varied temporal dynamics within a single, well-structured system. **Second**, we curate, preprocess and release an extensive and diverse corpus of medical time series, containing over 454 billion observations, to be used for model pre-training. This collection, built from multiple public datasets, is curated to cover diverse types of medical time series. We select data sources and control their proportions to reflect real-world variability, ensuring correct time alignment, consistent types, and high quality. **Third**, we establish a comprehensive benchmark suite that covers a wide range of clinical forecasting tasks. This suite allows for consistent evaluation of MIRA and future models, encouraging further research and development into robust and generalizable medical time series models.

2 Related Work

Medical Time Series Models. Machine learning has enabled significant progress in healthcare time series analysis, supporting a wide range of tasks, including dynamic forecasting [20, 21, 40, 41], survival analysis [42, 43], clustering and phenotyping [44–46], screening and monitoring [22, 47, 48], early diagnosis [23, 24, 49], pharmacology [50], treatment effect estimation [51, 52, 41], epidemiological and pandemic influenza surveillance [53], and hospital resource allocation [19, 54]. Despite this progress, most existing methods are narrowly designed for specific tasks or datasets, limiting their adaptability to diverse clinical scenarios [55]. Recently, foundation models for medical time series have emerged, showing promising cross-dataset generalization [33, 36, 34]. However, these models focus primarily on classification tasks and are not designed to handle continuous-time forecasting or irregular temporal patterns common in real-world clinical data.

Generalist Time Series Foundation Models. Recent foundation models have shown strong zero-shot forecasting without task-specific tuning [56–60]. Chronos [32] first adapted T5 [61] by discretizing time series intervals as text tokens. More recent models—Moirai [27], Sundial [31], and TimesFM [29]—improve support for variable dimensions and frequencies. Time-MoE [28] and Moirai-MoE [30] further improve specialization with sparse experts. However, these models largely require regularly sampled data, limiting their use on irregular clinical data. See Appendix A for more information.

Irregular Time Series Models. Modeling irregular time series has attracted increasing attention, particularly for applications requiring continuous-time reasoning. Early works such as Neural ODEs [39, 62] and State Space Models (SSMs)[63, 64] have demonstrated the ability to capture continuous dynamics by parameterizing the evolution of latent states over time. Another line of research focuses on adapting deep neural architectures, such as RNNs [65–67] and Transformers [18, 68–70], to irregular settings. While these models have shown success in tasks like interpolation and classification, their effectiveness for long-term forecasting remains underexplored.

3 Methodology

In this section, we discuss the architecture of MIRA. We first formalize the irregular medical time series forecasting task (Section 3.1). We then introduce the model architecture (Section 3.2). Finally, we present the pretraining corpus and training strategy (Section 3.3).

3.1 Irregular Medical Time Series Forecasting

Let each time series instance be represented as paired sequences of timestamps and observations: $\{(t_i, x_i)\}_{i=1}^N$ where $t_i \in \mathbb{R}^+$ are strictly increasing ($t_1 < \dots < t_N$) and $x_i \in \mathbb{R} \cup \{\text{NaN}\}$ contains real values or missing entries. Our model is designed to handle two prevalent irregular patterns: **(1) Regular-grid missing values.** Observations occur at *equidistant timestamps* $t_i = i\Delta t$ but with *time-level missing values*: some timestamps may have missing measurements. Formally, there exists a subset $\mathcal{M} \subseteq 1, \dots, N$ such that the corresponding observations x_i are missing (i.e., $x_i = \text{NaN}$) for all $i \in \mathcal{M}$, while the timestamps t_i remain fully observed. **(2) Irregular sampling.** Timestamps t_i follow *non-uniform intervals* with $\Delta t_i = t_{i+1} - t_i$ varying for different i . All observations at existing timestamps are present ($x_i \in \mathbb{R}$), but the temporal spacing is irregular. Adhering to the channel-independent setting [59], we formulate the problem in a uni-variate time series manner [27].

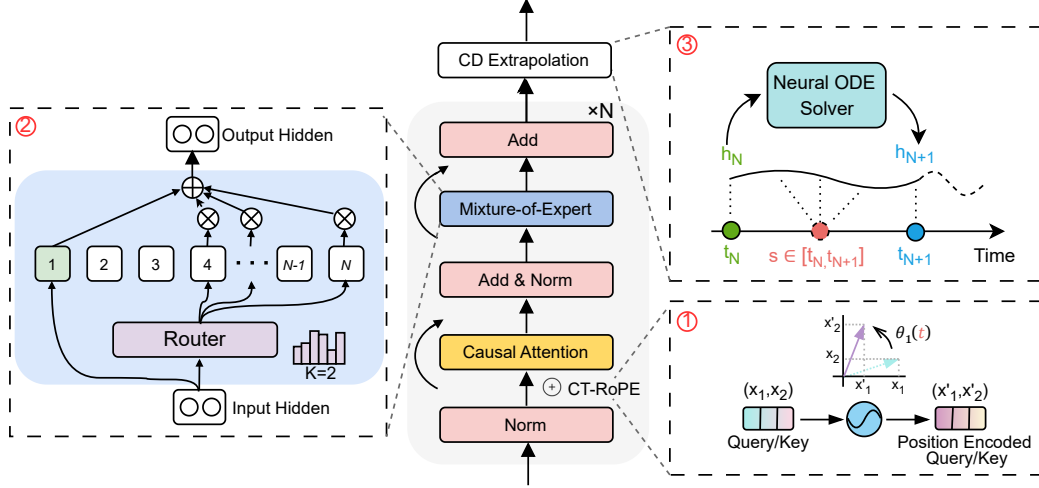


Figure 2: Architecture of **MIRA**. ① Takes irregular medical time series and timestamps as input, applying **CT-RoPE** for continuous temporal encoding. ② A **Sparse Temporal Mixture-of-Experts** layer routes tokens to specialized experts based on frequency. ③ A **Continuous Dynamics Extrapolation Block** evolves latent states toward arbitrary target timestamps for flexible time-aware forecasting.

Given history $\{(x_i, t_i)\}_{i=1}^L$, the forecasting task requires predicting future values at **known target timestamps** $\{t_{L+1}, \dots, t_{L+H}\}$:

$$\hat{\mathbf{x}}_{L+1:L+H} = f_{\theta}(\{(x_i, t_i)\}_{i=1}^L; \{t_j\}_{j=L+1}^{L+H}) \in \mathbb{R}^H \quad (1)$$

where $\{t_j\}_{j=L+1}^{L+H}$ may follow either regularity pattern.

3.2 Model Overview

We present **MIRA**, a decoder-only architecture for universal irregular medical time series forecasting. As illustrated in Figure 2, **MIRA** consists of three key components: (1) a Continuous-Time Rotary Positional Encoding, (2) a Sparse Temporal Mixture-of-Experts Module, and (3) a Continuous Dynamics Extrapolation Block. Together, they enable scalable, frequency-adaptive modeling of non-uniform clinical sequences.

3.2.1 Continuous-Time Rotary Positional Encoding

Standard RoPE [38] assumes discrete and uniformly spaced token indices, which limits its applicability to clinical time series with real-valued and irregular timestamps. To address this, we propose a *Continuous-Time Rotary Positional Encoding (CT-RoPE)* that generalizes RoPE to operate directly on continuous-time inputs. Let $t \geq 0$ denote the timestamp of a token in an irregularly sampled sequence, and let d be the model dimensionality, assumed to be even. Specifically, we discretize continuous timestamps $t \geq 0$ into rotation angles without assuming fixed intervals, enabling the model to handle irregular sampling (more detail can be found at Appendix B). The angular frequencies $\{\omega_i\}_{i=0}^{d/2-1}$ are defined as: $\omega_i = 10000^{-2i/d}$. The resulting time-dependent rotation angle is given by:

$$\theta_i(t) = \omega_i \cdot t \quad (2)$$

Given an input embedding $\mathbf{x} \in \mathbb{R}^d$, we partition it into $d/2$ two-dimensional sub-vectors (x_{2i}, x_{2i+1}) , and apply a planar rotation using the computed angle $\theta_i(t)$:

$$\begin{bmatrix} x'_{2i} \\ x'_{2i+1} \end{bmatrix} = \begin{bmatrix} \cos \theta_i(t) & -\sin \theta_i(t) \\ \sin \theta_i(t) & \cos \theta_i(t) \end{bmatrix} \begin{bmatrix} x_{2i} \\ x_{2i+1} \end{bmatrix} \quad (3)$$

CT-RoPE with Attention. The design of the rotary position encoding naturally supports relative position modeling. Specifically, the inner product between rotated query and key vectors depends only on the difference between their timestamps. This can be seen by expanding the attention score:

$$\langle q_m, k_n \rangle = x_m^\top (W^Q)^\top R_{\Theta, m}^\top R_{\Theta, n} W^K x_n \quad (4)$$

Since both $R_{\Theta, m}$ and $R_{\Theta, n}$ are rotation matrices constructed from trigonometric functions of the timestamp-derived angles, their product is itself a rotation matrix dependent only on the time difference:

$$R_{\Theta, m}^\top R_{\Theta, n} = R_{\Theta, n-m} \quad (5)$$

This implies that the positional interaction between two tokens is solely a function of their relative timestamp offset ($n - m$). In CT-RoPE, this property generalizes to real-valued timestamps, enabling the attention mechanism to capture continuous-time relational structure while retaining the efficiency and structure of standard dot-product attention. In line with Chowdhery et al. [71], we remove biases except in QKV projections to enhance extrapolation. More detail can be found in Appendix C.

3.2.2 Frequency-Specific Mixture-of-Experts Block

Medical time series often exhibit dynamics across multiple temporal frequencies, ranging from smooth long-term trends to rapid, short-term variations. To effectively capture such heterogeneity while maintaining computational efficiency, we adopt a sparse Mixture-of-Experts (MoE) architecture to replace the standard feedforward sub-layer in each Transformer block. In practice, each token is routed to a subset of K experts selected from a shared pool of N lightweight feedforward networks. These experts are parameterized independently and are intended to specialize in distinct temporal or semantic structures. Additionally, a *shared expert* is universally applied to all tokens, serving as a global residual pathway. Given the token representation $\bar{\mathbf{u}}_t^l \in \mathbb{R}^D$ at layer l , the output of the MoE block is calculated as:

$$\text{MoE}(\bar{\mathbf{u}}_t^l) = g_{N+1,t} \cdot \text{FFN}_{N+1}(\bar{\mathbf{u}}_t^l) + \sum_{i=1}^N g_{i,t} \cdot \text{FFN}_i(\bar{\mathbf{u}}_t^l), \quad (6)$$

where $\text{FFN}_i(\cdot)$ denotes the i -th expert network, $\text{FFN}_{N+1}(\cdot)$ the shared expert, and $g_{i,t}$, $g_{N+1,t}$ the corresponding routing weights. The non-shared expert weights $g_{i,t}$ are obtained via a softmax gating mechanism followed by top- K selection:

$$s_{i,t} = \frac{\exp((\mathbf{W}_i^l)^\top \bar{\mathbf{u}}_t^l)}{\sum_{j=1}^N \exp((\mathbf{W}_j^l)^\top \bar{\mathbf{u}}_t^l)}, \quad g_{i,t} = \begin{cases} s_{i,t}, & \text{if } s_{i,t} \in \text{TopK}(\{s_{j,t}\}_{j=1}^N, K), \\ 0, & \text{otherwise,} \end{cases} \quad (7)$$

where $\mathbf{W}_i^l \in \mathbb{R}^D$ are the trainable gating vectors. The shared expert weight $g_{N+1,t}$ is computed independently using a sigmoid gate:

$$g_{N+1,t} = \sigma((\mathbf{W}_{N+1}^l)^\top \bar{\mathbf{u}}_t^l), \quad (8)$$

where $\sigma(\cdot)$ denotes the element-wise sigmoid function and $\mathbf{W}_{N+1}^l \in \mathbb{R}^D$ is the shared expert gating vector.

3.2.3 Continuous Dynamics Extrapolation Block

Auto-regressive transformer architectures, which generate predictions in a stepwise manner under causal masking, cannot incorporate the timestamp of the target token during inference, as it is not available until after generation. To address this limitation and enable extrapolation to arbitrary timestamps, we introduce a Neural ODE-based [39] extrapolation module that evolves the latent state from the current token’s timestamp to the target prediction token timestamp, allowing time-aware forecasting at unseen or irregular time points.

Given $h(t_N) \in \mathbb{R}^d$ (the state at time t_N) and the next target timestamp t_{N+1} , the Neural ODE module extrapolates h_N to $h(t_{N+1})$. We define the temporal evolution of the hidden state $h(s)$ over the interval $s \in [t_N, t_{N+1}]$ as:

$$\frac{dh(s)}{ds} = f(s - t_N, h(s); \theta_{ODE}), \quad h(t_N) = h_N, \quad \text{for } s \in [t_N, t_{N+1}] \quad (9)$$

where $f : \mathbb{R}_{\geq 0} \times \mathbb{R}^{D_{model}} \rightarrow \mathbb{R}^{D_{model}}$ is the dynamics function, parameterized by a neural network (e.g., an MLP) with parameters θ_{ODE} . f takes the relative time $\Delta s = s - t_N$ and the current state $h(s)$ as input. The state at the target time t_{N+1} is obtained by integrating the ODE dynamics:

$$h(t_{N+1}) = h_N + \int_{t_N}^{t_{N+1}} f(s - t_N, h(s); \theta_{ODE}) ds \quad (10)$$

This integral is computed numerically using an ODE solver (i.e. the Dormand-Prince (RK45) method). Let the result of this numerical integration be denoted as $h'_{N+1} = h(t_{N+1})$. More detail is in Appendix D.

Implementation with Adaptive ODE Solvers We numerically approximate the solution to Equation 10 using adaptive step-size ODE solvers. Appropriate absolute and relative error tolerances (e.g., 10^{-6}) are set to manage the trade-off between accuracy and computational cost.

3.3 Model Training

Medical Pretraining Dataset. To support generalizable and clinically relevant time series modeling, we curate a large pretraining corpus spanning over 454 billion time points from various real-world healthcare settings. The dataset collection includes signals from ICUs and operating rooms, pediatric critical care, long-term sleep and mental health monitoring, and population-level epidemiological surveillance. All data are drawn from publicly available clinical datasets, including MIMIC-III [72], MIMIC-IV [73], PTB-XL [74], Sleep-EDF [75], and the WAVES Pediatric Waveform Database [76]. A full summary of included datasets and the pre-processing applied is provided in Appendix E.

Loss Function. Training large-scale medical time series models requires balancing predictive accuracy, numerical stability, and sparse expert utilization. To ensure robustness against outliers and noisy measurements common in clinical data, we employ the Huber loss $\mathcal{L}_{\text{Huber}}$ over autoregressive multi-horizon predictions:

$$\mathcal{L}_{\text{Huber}}(x, \hat{x}) = \begin{cases} \frac{1}{2}(x - \hat{x})^2, & \text{if } |x - \hat{x}| \leq \delta, \\ \delta \cdot (|x - \hat{x}| - \frac{1}{2}\delta), & \text{otherwise,} \end{cases} \quad (11)$$

where δ is a threshold controlling the transition between L2 and L1 loss regimes. To avoid expert collapse in the sparse MoE layer, we introduce a load balancing loss \mathcal{L}_{aux} that promotes uniform usage of experts. Let f_i be the fraction of tokens assigned to expert i , and r_i the average routing probability:

$$\mathcal{L}_{\text{aux}} = N \cdot \sum_i f_i r_i, \quad (12)$$

where $f_i = \frac{1}{KT} \sum_{t=1}^T \mathbb{I}(\text{Expert } i \text{ selected at } t)$ and $r_i = \frac{1}{T} \sum_{t=1}^T s_{i,t}$ with $s_{i,t}$ being the softmax routing score.

Table 1: A high-level summary of MIRA model configurations.

	Layers	Experts	K	d_{model}	d_{ff}	d_{expert}	Activated Params	Total Params
<i>MIRA_{small}</i>	8	8	2	288	1152	144	30 M	73 M
<i>MIRA_{base}</i>	12	8	2	384	1536	192	50 M	114 M
<i>MIRA_{large}</i>	12	8	2	768	3072	384	200 M	455 M

Model Configurations. We adopt a similar model configuration strategy following Time-MoE [28] by providing three model variants of increasing scale: $MIRA_{small}$, with approximately 73 million parameters; $MIRA_{base}$, with approximately 114 million parameters; $MIRA_{large}$, with approximately 455 million parameters; All models are trained on max to eight NVIDIA 80G H/A100 GPUs, using a micro batch size of 128, and a maximum sequence length of 512. For model configurations and training details, refer to Appendix F.

4 Experiments

In this section, we present the empirical evaluation of MIRA. We begin by outlining the experimental setup (Section 4.1). We then evaluate MIRA on zero-shot forecasting benchmarks under both out-of-distribution (Section 4.2) and in-distribution (Section 4.3) settings. Additionally, we analyze the model’s scaling behavior across varying model and dataset sizes, and evaluate its robustness to different levels of data irregularity (Section 4.4). Finally, we conduct ablation studies to examine what contributes to MIRA’s performance (Section 4.5).

4.1 Experiment Setup

Downstream Clinical Datasets. We evaluate MIRA on a diverse suite of real-world clinical and public health datasets, spanning multi-modal physiological signal analysis, critical care monitoring, ambulatory bio-signal tracking, epidemiological surveillance, pharmacological safety, and healthcare resource utilization. To systematically study temporal robustness, we group datasets into two categories: (1) *inherently irregular* datasets, which exhibit irregular sampling and natural missing values due to clinical or observational workflows. These are CinC 2012 [77] and CinC 2019 [78]. Furthermore, we use (2) *originally regular* datasets, i.e., MIT-BIH [79], Johns Hopkins COVID-19 Dataset [80], CDC Influenza Hospitalizations Admissions (CDC-IHA)¹, WHO fluent², Heart Rate [81] and illness [82], for which we simulate irregularity by randomly masking 30% of time points. The full list of datasets and statistics is provided in Appendix G.

Baselines. We compare MIRA against 13 state-of-the-art forecasting models, which we categorize into three groups: (i) zero-shot foundation models, including Time-MoE [28]³, Moirai [27], Moirai-MoE [30], Moment [83], TimeGPT [84], Timer [85], Lag-Llama [86], TimesFM [29], and Chronos [32], which require inputs to be interpolated for evaluation; and (ii) full-shot forecasting models, including ContiFormer [18], T-PatchGNN [87], Neural-CDE [88], and ODE-RNN [65], which are specialized for irregularly sampled time series and require task-specific training. (iii) Continue pre-trained zero-shot foundation models on medical corpora, including Time-MoE [28], Moirai [27] and Chronos [32] which performance best on zero-shot evaluation. Implementation details for all baselines are provided in Appendix H.

Evaluation Metrics. We measure the Root Mean Squared Error (RMSE) and the Mean Absolute Error (MAE) as the evaluation metrics. Detailed definitions are provided in Appendix I.

4.2 Performance on Out-of-distribution Forecasting

Objective. We evaluated seven unseen benchmarks excluded from pre-training corpora. For comparison, we fine-tuned the *full-shot forecasting models* on the training split of each benchmark, while the *zero-shot foundation models* were evaluated directly without any task-specific training or fine-tuning. To validate the effectiveness of our model architecture, we additionally pre-trained existing foundation models on the same medical corpus. Notably, *CINC 2012* and *CINC 2019* were excluded from this evaluation for foundation models, as applying regular-grid interpolation at the finest resolution results in over 98% of time steps being interpolated, leading to poor performance for all baselines.

Results. Detailed results of out-of-distribution performance are reported in Table 2. First, **MIRA consistently achieves state-of-the-art performance**, outperforming all general-domain foundation models and specialized time series baselines. Specifically, $MIRA_{large}$ achieves the best results on all datasets, improving RMSE by over 10% on average compared to the strongest baselines, confirming

¹<https://www.cdc.gov/flu-forecasting/data-vis/current-week.html>

²<https://www.who.int/tools/flunet>

³We excluded Time-MoE Ultra and Sundial from baselines as they are not open-sourced.

Table 2: Zero-shot forecasting performance on out-of-distribution datasets that are regularly sampled but contain missing values. Reported values are averaged across all prediction lengths. Lower RMSE and MAE indicate better predictions. **Red**: the best; **Blue**: the second best compared to zero-shot baselines; **Underline**: the best performance compared to full-shot baselines.

Models	Zero-shot Ours						Full-shot Time Series Models									
	MIRA _{small}		MIRA _{base}		MIRA _{large}		Contiformer		T-PatchGNN		ODE-RNN		Neural-CDE		TimesFM	
	RMSE	MAE	RMSE	MAE	RMSE	MAE	RMSE	MAE	RMSE	MAE	RMSE	MAE	RMSE	MAE	RMSE	MAE
Cinc 2012 (10 ¹)	5.963	5.891	5.764	5.732	<u>5.312</u>	<u>5.120</u>	5.987	5.985	6.247	6.246	6.997	6.995	7.498	7.497	-	-
Cinc 2019 (10 ¹)	7.456	6.597	7.347	7.311	7.212	7.246	6.989	<u>7.072</u>	7.608	7.541	10.293	9.7724	9.591	8.322	-	-
Heart Rate (10 ⁻⁵)	1.195	1.001	1.123	0.950	0.986	0.845	0.774	0.633	0.627	<u>0.497</u>	0.945	0.683	0.671	0.587	1.753	0.832
MIT-BIH	0.293	0.198	0.163	0.111	0.122	0.091	0.453	0.354	0.705	0.627	0.882	0.623	0.242	0.196	0.335	0.141
CDC-IHA (10 ¹)	5.976	4.684	5.729	4.502	5.534	4.401	5.510	<u>4.133</u>	9.522	7.974	10.068	9.052	7.892	6.766	15.633	4.408
JH COVID-19 (10 ²)	0.407	0.355	0.504	0.349	0.478	0.336	0.323	<u>0.297</u>	0.350	0.291	0.424	0.331	0.545	0.503	2.329	0.322
ILI	1.294	1.077	1.218	1.024	1.114	0.926	0.391	0.224	<u>0.195</u>	<u>0.143</u>	0.410	0.264	0.423	0.314	2.034	1.333
1st Count	0	0	0	0	4	3	0	0	0	0	0	0	0	0	0	0
Zero-shot Foundation Models Pre-trained on General-domain Corpora																
Baseline	Lag-Llama		TimeGPT		Timer		Moment _{small}		Moment _{base}		Moment _{large}		Moirai-MoE _{small}		Moirai-MoE _{base}	
	RMSE	MAE	RMSE	MAE	RMSE	MAE	RMSE	MAE	RMSE	MAE	RMSE	MAE	RMSE	MAE	RMSE	MAE
Heart Rate (10 ⁻¹)	1.764	1.488	2.258	1.915	1.901	1.704	2.966	1.852	2.939	1.835	2.917	1.735	1.982	1.600	2.144	1.652
MIT-BIH	0.217	0.169	0.231	0.185	0.255	0.213	0.417	0.229	0.416	0.228	0.413	0.224	0.208	0.167	0.208	0.167
CDC-IHA (10 ¹)	6.531	4.846	6.654	4.860	6.424	4.857	17.803	5.307	17.631	5.288	17.689	5.260	7.099	5.405	7.639	5.862
JH COVID-19 (10 ²)	3.596	1.432	1.879	1.580	2.647	2.328	3.077	0.553	3.097	0.554	3.064	0.549	1.452	0.725	19.391	3.190
ILI	1.780	1.366	2.011	1.077	1.882	1.492	1.570	1.056	1.566	1.054	1.566	1.052	2.001	1.678	1.983	1.664
1st Count	0	0	0	0	0	0	0	0	0	0	0	0	0	0	0	0
Zero-shot Foundation Models Pre-trained on General-domain Corpora																
Baseline	Moirai _{small}		Moirai _{base}		Moirai _{large}		Time-MoE _{base}		Time-MoE _{large}		Chronos _{small}		Chronos _{base}		Chronos _{large}	
	RMSE	MAE	RMSE	MAE	RMSE	MAE	RMSE	MAE	RMSE	MAE	RMSE	MAE	RMSE	MAE	RMSE	MAE
Heart Rate (10 ⁻¹)	2.359	1.965	2.156	1.767	2.098	1.644	0.850	0.650	0.833	0.639	1.357	0.587	1.189	0.489	1.218	0.506
MIT-BIH	0.343	0.249	0.421	0.302	0.593	0.149	0.171	0.135	0.172	0.135	0.353	0.147	0.361	0.149	0.350	0.147
CDC-IHA (10 ¹)	6.835	5.271	7.328	5.526	6.788	5.302	6.311	4.748	6.312	4.715	15.502	4.421	15.825	4.438	15.986	4.517
JH COVID-19 (10 ²)	1.917	0.695	0.991	0.474	0.614	0.402	0.596	0.402	0.512	0.371	4.826	1.031	3.835	0.551	3.478	0.521
ILI	1.995	1.671	1.871	1.561	1.808	1.499	1.288	0.951	1.366	1.015	2.054	1.400	1.940	1.308	1.870	1.252
1st Count	0	0	0	0	0	0	0	0	0	0	0	0	0	0	0	0
Zero-shot Foundation Models Continue Pre-trained on Medical Corpora																
Baseline	Moirai _{small}		Moirai _{base}		Moirai _{large}		Time-MoE _{base}		Time-MoE _{large}		Chronos _{small}		Chronos _{base}		Chronos _{large}	
	RMSE	MAE	RMSE	MAE	RMSE	MAE	RMSE	MAE	RMSE	MAE	RMSE	MAE	RMSE	MAE	RMSE	MAE
Heart Rate (10 ⁻¹)	2.047	1.685	1.907	1.536	1.601	1.263	0.648	0.524	0.603	0.488	1.049	0.555	0.965	0.488	0.902	0.458
MIT-BIH	0.239	0.204	0.274	0.190	0.219	0.176	0.132	0.103	0.131	0.101	0.311	0.137	0.320	0.139	0.306	0.127
CDC-IHA (10 ¹)	6.690	5.310	6.934	5.376	6.696	5.114	6.327	4.698	6.299	4.666	14.502	4.321	14.825	4.338	14.986	4.417
JH COVID-19 (10 ²)	0.579	0.448	0.619	0.478	0.812	0.337	0.509	0.353	0.517	0.362	4.225	0.947	3.535	0.510	3.328	0.469
ILI	1.528	1.289	1.435	1.191	1.501	1.229	1.188	0.915	1.201	0.927	1.705	1.127	1.639	1.081	1.547	1.028
1st Count	0	0	0	0	0	0	0	1	1	1	0	0	0	0	0	0

the advantage of scaling and medical pretraining. This advantage is particularly pronounced on clinical benchmarks such as MIT-BIH and CDC-IHA, where MIRA_{large} achieves both the lowest RMSE and MAE. Second, **domain-specific pretraining proves essential**. All model variants—continue pretrained on medical corpora—consistently outperform models trained on general time series data. This demonstrates the benefit of leveraging medical-specific temporal structures and distributions during pretraining. Interestingly, even smaller MIRA models surpass larger general-domain models, suggesting that data relevance is more critical than model size alone. Third, **MIRA achieves performance close to or even exceeding fine-tuned full-shot models in several cases**. For instance, MIRA_{large} outperform than full-shot baseline on Cinc 2012 and slight lower in JH Covid-19.

4.3 Performance on In-distribution Forecasting

Objective. We evaluated in-distribution performance by holding out a portion of the pre-training datasets as test sets, ensuring no data leakage. All models were tested in zero-shot settings.

Results. As shown in Table 3, MIRA consistently achieves highly competitive zero-shot performance across all five pre-training datasets. Compared to baselines such as Moirai, Time-MoE, and Chronos, MIRA demonstrates lower RMSE and MAE on most datasets, particularly excelling on PTB-XL, MIMIC-III, and MIMIC-IV. This advantage holds across all model scales, indicating stable scalability and generalization. In contrast, baselines show larger variance or degradation on challenging datasets with missing values. These results validate the robustness of MIRA’s architecture in handling imperfect medical time series data without requiring task-specific adaptation.

Table 3: Zero-shot forecasting performance on out-of-distribution datasets that are regularly sampled but contain missing values. Reported values are averaged across all prediction lengths. Lower RMSE and MAE indicate better predictions. **Red**: the best; **Blue**: the second best.

Models	Zero-shot Ours			Zero-shot Baseline								
	MIRA _{small}	MIRA _{base}	MIRA _{large}	Moirai _{small}	Moirai _{base}	Moirai _{large}	Time-MoE _{base}	Time-MoE _{large}	Chronos _{small}	Chronos _{base}	Chronos _{large}	
RMSE	SleepEDF (10 ²)	0.215	0.195	0.189	0.301	0.668	0.304	0.228	0.244	0.411	0.414	0.413
	PTB-XL	0.147	0.127	0.121	0.177	0.270	0.416	0.110	0.109	0.228	0.234	0.229
	MIMIC-III	0.126	0.107	0.102	0.163	0.256	0.172	0.105	0.103	0.153	0.154	0.151
	MIMIC-IV	0.111	0.091	0.081	0.259	0.300	0.319	0.084	0.082	0.309	0.317	0.319
	WAVES	0.154	0.136	0.129	0.177	0.190	0.169	0.148	0.141	0.184	0.183	0.182
	1 st Count	0	4	4	0	0	0	0	1	0	0	0
MAE	SleepEDF (10 ²)	0.180	0.162	0.156	0.264	0.227	0.323	0.191	0.203	0.192	0.193	0.193
	PTB-XL	0.110	0.095	0.091	0.125	0.098	0.099	0.063	0.066	0.100	0.104	0.103
	MIMIC-III	0.106	0.089	0.084	0.141	0.164	0.138	0.081	0.078	0.079	0.080	0.080
	MIMIC-IV	0.094	0.069	0.061	0.223	0.291	0.143	0.064	0.062	0.134	0.142	0.143
	WAVES	0.129	0.112	0.106	0.157	0.181	0.155	0.124	0.116	0.119	0.118	0.117
	1 st Count	0	0	3	0	0	0	1	1	0	0	0

Table 4: Zero-shot forecasting performance on different missing rates. Reported values are averaged across all prediction lengths. Lower RMSE and MAE indicate better predictions. **Red**: the best; **Blue**: the second best.

Missing Rate	10%+		20%+		30%+		40%+		50%+		60%+		70%+		80%+		90%+		1 st Count		
	RMSE	MAE	RMSE	MAE	RMSE	MAE	RMSE	MAE	RMSE	MAE	RMSE	MAE	RMSE	MAE	RMSE	MAE	RMSE	MAE	RMSE	MAE	
Ours	MIRA _{small}	3.15	2.82	3.28	2.95	3.41	3.08	3.54	3.20	3.67	3.34	3.80	3.47	3.93	3.61	4.07	3.75	4.22	3.90	0	0
	MIRA _{base}	2.98	2.68	3.11	2.81	3.25	2.94	3.38	3.07	3.51	3.20	3.64	3.34	3.78	3.48	3.93	3.63	4.10	3.79	0	1
	MIRA _{large}	2.85	2.56	2.95	2.65	3.08	2.78	3.21	2.90	3.35	3.04	3.49	3.18	3.63	3.31	3.99	3.86	3.97	3.64	8	8
	Time-MoE _{base}	3.05	2.78	3.18	2.92	3.32	3.05	3.45	3.18	3.58	3.31	3.71	3.43	3.85	3.57	3.99	3.71	4.15	3.86	0	0
	Time-MoE _{large}	3.20	2.91	3.33	3.04	3.47	3.17	3.60	3.29	3.73	3.41	3.86	3.54	3.99	3.67	4.13	3.81	4.28	3.96	0	0
	Moirai _{large}	4.80	4.18	5.39	4.64	5.68	4.55	6.02	4.83	6.09	5.06	6.18	5.02	6.31	5.09	6.51	5.24	6.71	5.36	0	0
	Moirai _{base}	4.84	4.15	4.93	4.10	5.20	4.23	5.64	4.53	5.78	4.61	5.80	4.60	5.95	4.97	5.95	4.73	6.06	4.87	0	0
	Moirai _{small}	4.91	4.22	5.04	4.20	6.12	4.93	6.23	4.98	6.44	5.49	6.47	5.18	6.59	5.60	6.66	5.20	6.86	5.71	0	0
	Chronos _{large}	4.71	4.10	4.85	4.22	5.02	4.31	5.31	4.52	5.58	4.70	5.82	4.91	5.97	5.10	6.15	5.32	6.43	5.49	0	0
	Chronos _{base}	5.02	4.40	5.21	4.51	5.43	4.68	5.62	4.81	5.85	4.93	6.02	5.12	6.21	5.31	6.40	5.49	6.67	5.62	0	0
	Chronos _{small}	5.32	4.71	5.49	4.82	5.68	4.93	5.81	5.02	6.01	5.20	6.21	5.32	6.40	5.49	6.58	5.61	6.83	5.72	0	0
	Time-MoE _{base}	2.95	2.70	3.08	2.83	3.22	2.96	3.35	3.09	3.48	3.22	3.61	3.35	3.75	3.49	3.89	3.63	4.04	3.78	1	0
Time-MoE _{large}	3.05	2.78	3.18	2.91	3.32	3.04	3.45	3.17	3.58	3.30	3.71	3.43	3.85	3.57	3.99	3.71	4.15	3.86	0	0	
Medical Setting	Moirai _{large}	4.41	3.76	4.92	4.20	5.35	4.41	5.69	4.76	5.93	4.80	6.09	4.92	6.23	4.98	6.48	5.29	6.62	5.30	0	0
	Moirai _{base}	4.55	3.92	4.78	4.07	5.18	4.26	5.49	4.46	5.78	4.64	5.70	4.51	5.87	4.97	5.92	4.75	5.96	4.71	0	0
	Moirai _{small}	5.02	4.21	5.36	4.40	5.55	4.98	5.97	4.92	6.25	5.34	6.43	5.11	6.44	5.35	6.57	5.41	6.58	5.30	0	0
	Chronos _{large}	4.30	3.89	4.58	4.02	4.83	4.20	5.02	4.31	5.32	4.51	5.61	4.73	5.83	4.91	6.02	5.10	6.31	5.32	0	0
	Chronos _{base}	4.61	4.10	4.83	4.20	5.02	4.31	5.32	4.51	5.58	4.70	5.82	4.91	5.97	5.10	6.15	5.32	6.43	5.49	0	0
	Chronos _{small}	4.83	4.31	5.02	4.43	5.32	4.51	5.58	4.70	5.82	4.91	5.97	5.10	6.15	5.32	6.43	5.49	6.71	5.61	0	0

4.4 Model Scaling and Data Behavior.

Objective. We investigate the robustness of the MIRA by comparing performance with baselines under varying missing datarates on the WHO FluNet dataset which is not used in pre-training.

Data Behavior Result. Table 4 summarizes the zero-shot forecasting performance under varying missing rates, ranging from 10% to 90%. MIRA consistently outperforms all baselines across all missing rates, with $MIRA_{large}$ achieving the lowest RMSE and MAE in nearly every setting. Notably, $MIRA_{large}$ maintains strong performance even as the missing rate increases, showing minimal performance degradation compared to other models. This demonstrates its robustness to severe information loss. While $Time - MoE_{large}$ performs competitively at lower missing rates, its performance drops more quickly as missingness increases.

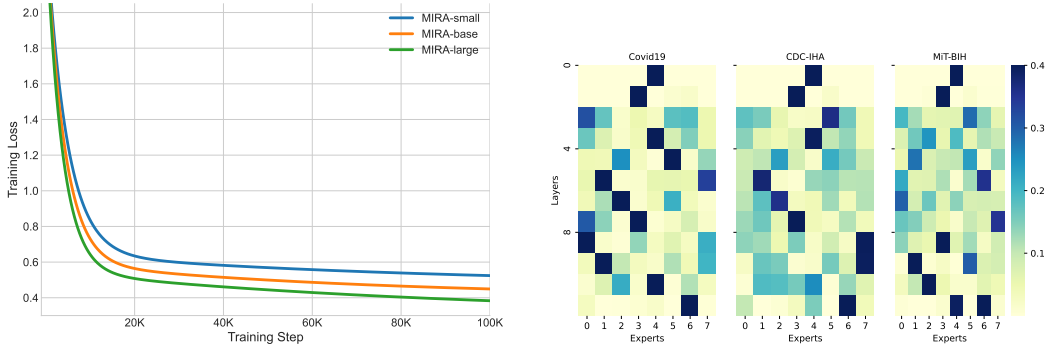
Pretraining Scalability. Beyond downstream performance, we delve into the utilization of model capacity. We plot training curves in Figure 3. Compared with small size, the large version leads to totally 11% reduction in the converged training objective, showing significant performance promotion on in-distribution medical time series forecasting.

4.5 Ablation Analysis

Objective. We further perform an ablation study by removing key components of MIRA, to quantify their contribution, and the impact of the number of experts on performance.

Component Ablation Results. As shown in the left-hand side of Table 5, removing CT-RoPE (w/o CT-RoPE) leads to a performance drop, confirming the importance of our continuous-time positional encoding. Similarly, eliminating the Mixture-of-Experts block (w/o MoE Block) slightly degrades performance, showing the value of expert specialization. The largest degradation is observed when disabling the CT-Extrapolation Block, with RMSE and MAE increasing by 5 and 8%, respectively,

Figure 3: **(Left)** Training curves on Medical corpora of different MIRA model sizes. **(Right)** Gating scores for experts across different layers in the three different frequency datasets.



highlighting its role in improving extrapolation. These results showcase the complementary benefits of all three components in achieving robust performance.

Table 5: Ablation studies. **(Left)** Evaluated with different model components. **(Right)** Analysis performance and inference speed across different top_k setups. Lower values indicate better performance.

Component	RMSE	MAE	Top _k Setup	RMSE	MAE	Speed (s/iter)
<i>MIRA</i> _{base}	0.154	0.118	w/ {Top ₁ }	0.160	0.121	0.097
w/o CT-RoPE	0.158	0.125	w/ {Top ₂ }	0.154	0.118	0.101
w/o MoE Block	0.157	0.122	w/ {Top ₄ }	0.154	0.117	0.112
w/o CT-Extrapolation Block	0.162	0.128	w/ {Top ₆ }	0.156	0.120	0.124
			w/ {Top ₈ }	0.159	0.122	0.127

Expert Activation Analysis. We further examine the trade-off between predictive performance and inference efficiency by varying the number of activated experts (top_k), as shown in the right-hand side of Table 5. Activating two experts (top_2) achieves the best balance, reaching the lowest RMSE of 0.154 with an inference speed of 0.101 s/iter. Increasing to four experts provides no meaningful improvement in performance but increases inference time to 0.112 s/iter. Further increasing to six or eight experts leads to slower inference with diminishing returns. Conversely, using a single expert (top_1) sacrifices accuracy (0.160) for only a marginal speed gain. These findings indicate that using two experts offers an optimal trade-off between efficiency and accuracy for scalable deployment.

Activation Visualization.

We further visualize expert activation patterns on three datasets with distinct temporal resolutions: MIT-BIH (high-frequency, Hz-level), CDC-IHA (weekly), and COVID-19 (daily). As shown in Figure 3, low-frequency datasets such as Covid19 dataset tend to activate a different set of experts compared to the high-frequency MIT-BIH dataset.

5 Discussion & Conclusion

We introduce **MIRA**, a foundation model designed for medical time series forecasting under irregular conditions. By integrating CT-RoPE, a Time-Specialized MOE module, and Continuous Dynamics Extrapolation, MIRA demonstrates strong generalization capabilities across diverse medical datasets. This work highlights the potential of scalable and temporally adaptive solutions to real-world medical challenges.

Limitation. This work is based on publicly available, de-identified medical datasets. While these resources offer broad coverage and ensure reproducibility, they may not fully reflect the complexities of real-world clinical deployment. In addition, although these datasets are anonymized, residual privacy risks may still exist; however, addressing such risks lies beyond the scope of this work.

References

- [1] Utkarsh Gupta, Naveen Paluru, Deepankar Nankani, Kanchan Kulkarni, and Navchetan Awasthi. A comprehensive review on efficient artificial intelligence models for classification of abnormal cardiac rhythms using electrocardiograms. *Heliyon*, 2024.
- [2] Vijay Ekambaram, Arindam Jati, Nam Nguyen, Phanwadee Sinthong, and Jayant Kalagnanam. Tsmixer: Lightweight mlp-mixer model for multivariate time series forecasting. In *Proceedings of the 29th ACM SIGKDD conference on knowledge discovery and data mining*, pages 459–469, 2023.
- [3] Mike Van Ness, Huibin Shen, Hao Wang, Xiaoyong Jin, Danielle C Maddix, and Karthick Gopalswamy. Cross-frequency time series meta-forecasting. *arXiv preprint arXiv:2302.02077*, 2023.
- [4] Bowen Deng, Chang Xu, Hao Li, Yuhao Huang, Min Hou, and Jiang Bian. Tardiff: Target-oriented diffusion guidance for synthetic electronic health record time series generation. *CoRR*, abs/2504.17613, 2025.
- [5] Hrayr Harutyunyan, Hrant Khachatryan, David C. Kale, and Aram Galstyan. Multitask learning and benchmarking with clinical time series data. *CoRR*, abs/1703.07771, 2017.
- [6] Lin Lawrence Guo, Ethan Steinberg, Scott Lanyon Fleming, Jose Posada, Joshua Lemmon, Stephen R Pfohl, Nigam Shah, Jason Fries, and Lillian Sung. Ehr foundation models improve robustness in the presence of temporal distribution shift. *Scientific Reports*, 13(1):3767, 2023.
- [7] Yuxi Liu, Zhenhao Zhang, Antonio Jimeno-Yepes, and Flora D. Salim. Modeling long-term dependencies and short-term correlations in patient journey data with temporal attention networks for health prediction. In *BCB*, pages 16:1–16:10. ACM, 2022.
- [8] Yizhi Li, Ge Zhang, Xingwei Qu, Jiali Li, Zhaoqun Li, Zekun Wang, Hao Li, Ruibin Yuan, Yinghao Ma, Kai Zhang, et al. Cif-bench: A chinese instruction-following benchmark for evaluating the generalizability of large language models. *arXiv preprint arXiv:2402.13109*, 2024.
- [9] Berkman Sahiner, Weijie Chen, Ravi K Samala, and Nicholas Petrick. Data drift in medical machine learning: implications and potential remedies. *The British Journal of Radiology*, 96(1150):20220878, 2023.
- [10] Lin Lawrence Guo, Stephen R Pfohl, Jason Fries, Alistair EW Johnson, Jose Posada, Catherine Aftandilian, Nigam Shah, and Lillian Sung. Evaluation of domain generalization and adaptation on improving model robustness to temporal dataset shift in clinical medicine. *Scientific reports*, 12(1):2726, 2022.
- [11] Viktor Schlegel, Hao Li, Yuping Wu, Anand Subramanian, Thanh-Tung Nguyen, Abhinav Ramesh Kashyap, Daniel Beck, Xiao-Jun Zeng, Riza Theresa Batista-Navarro, Stefan Winkler, and Goran Nenadic. PULSAR at mediqa-sum 2023: Large language models augmented by synthetic dialogue convert patient dialogues to medical records. In *CLEF (Working Notes)*, volume 3497 of *CEUR Workshop Proceedings*, pages 1668–1679. CEUR-WS.org, 2023.
- [12] He Li, Lu Yu, and Wu He. The impact of gdpr on global technology development, 2019.
- [13] Hao Li, Yuping Wu, Viktor Schlegel, Riza Batista-Navarro, Thanh-Tung Nguyen, Abhinav Ramesh Kashyap, Xiao-Jun Zeng, Daniel Beck, Stefan Winkler, and Goran Nenadic. Team: PULSAR at probsum 2023: PULSAR: pre-training with extracted healthcare terms for summarising patients’ problems and data augmentation with black-box large language models. In *BioNLP@ACL*, pages 503–509. Association for Computational Linguistics, 2023.
- [14] Yuting He, Fuxiang Huang, Xinrui Jiang, Yuxiang Nie, Minghao Wang, Jiguang Wang, and Hao Chen. Foundation model for advancing healthcare: Challenges, opportunities, and future directions. *CoRR*, abs/2404.03264, 2024.
- [15] Yuqi Nie, Nam H. Nguyen, Phanwadee Sinthong, and Jayant Kalagnanam. A time series is worth 64 words: Long-term forecasting with transformers. In *ICLR*. OpenReview.net, 2023.

- [16] Paul Pöhl, Viktor Schlegel, Hao Li, and Anil Bharath. Generating realistic multi-beat eeg signals. *arXiv preprint arXiv:2505.18189*, 2025.
- [17] Zachary C. Lipton, David C. Kale, and Randall C. Wetzell. Directly modeling missing data in sequences with rnns: Improved classification of clinical time series. In *MLHC*, volume 56 of *JMLR Workshop and Conference Proceedings*, pages 253–270. JMLR.org, 2016.
- [18] Yuqi Chen, Kan Ren, Yansen Wang, Yuchen Fang, Weiwei Sun, and Dongsheng Li. Contiformer: Continuous-time transformer for irregular time series modeling. In *NeurIPS*, 2023.
- [19] Lin Wang, Zheng Yin, Mamta Puppala, Chika F. Ezeana, Kelvin K. Wong, Tiancheng He, Deepa B. Gotur, and Stephen T. C. Wong. A time-series feature-based recursive classification model to optimize treatment strategies for improving outcomes and resource allocations of COVID-19 patients. *IEEE J. Biomed. Health Informatics*, 26(7):3323–3329, 2022.
- [20] Thomas Ferté, Dan Dutartre, Boris P. Hejblum, Romain Griffier, Vianney Jouhet, Rodolphe Thiébaud, Pierrick Legrand, and Xavier Hinaut. Reservoir computing for short high-dimensional time series: an application to sars-cov-2 hospitalization forecast. In *ICML*. OpenReview.net, 2024.
- [21] Jiayuan Chen, Changchang Yin, Yuanlong Wang, and Ping Zhang. Predictive modeling with temporal graphical representation on electronic health records. In *IJCAI*, pages 5763–5771. ijcai.org, 2024.
- [22] Ziyu Jia, Xihao Yang, Chenyang Zhou, Haoyang Deng, and Tianzi Jiang. ATTA: adaptive test-time adaptation for multi-modal sleep stage classification. In *IJCAI*, pages 5882–5890. ijcai.org, 2024.
- [23] Zhi Zhang, Shenghua Zhong, and Yan Liu. Beyond mimicking under-represented emotions: Deep data augmentation with emotional subspace constraints for eeg-based emotion recognition. In *AAAI*, pages 10252–10260. AAAI Press, 2024.
- [24] Hyunwoo Sohn, Kyungjin Park, Baekkwon Park, and Min Chi. Multi-ta: Multilevel temporal augmentation for robust septic shock early prediction. In *IJCAI*, pages 6035–6043. ijcai.org, 2024.
- [25] Xue Yang, Xuejun Qi, and Xiaobo Zhou. Deep learning technologies for time series anomaly detection in healthcare: A review. *IEEE Access*, 11:117788–117799, 2023.
- [26] Yuxuan Liang, Haomin Wen, Yuqi Nie, Yushan Jiang, Ming Jin, Dongjin Song, Shirui Pan, and Qingsong Wen. Foundation models for time series analysis: A tutorial and survey. In *KDD*, pages 6555–6565. ACM, 2024.
- [27] Gerald Woo, Chenghao Liu, Akshat Kumar, Caiming Xiong, Silvio Savarese, and Doyen Sahoo. Unified training of universal time series forecasting transformers. In *ICML*. OpenReview.net, 2024.
- [28] Xiaoming Shi, Shiyu Wang, Yuqi Nie, Dianqi Li, Zhou Ye, Qingsong Wen, and Ming Jin. Time-moe: Billion-scale time series foundation models with mixture of experts. *CoRR*, abs/2409.16040, 2024.
- [29] Abhimanyu Das, Weihao Kong, Rajat Sen, and Yichen Zhou. A decoder-only foundation model for time-series forecasting. In *ICML*. OpenReview.net, 2024.
- [30] Xu Liu, Juncheng Liu, Gerald Woo, Taha Aksu, Yuxuan Liang, Roger Zimmermann, Chenghao Liu, Silvio Savarese, Caiming Xiong, and Doyen Sahoo. Moirai-moe: Empowering time series foundation models with sparse mixture of experts. *CoRR*, abs/2410.10469, 2024.
- [31] Yong Liu, Guo Qin, Zhiyuan Shi, Zhi Chen, Caiyin Yang, Xiangdong Huang, Jianmin Wang, and Mingsheng Long. Sundial: A family of highly capable time series foundation models. *CoRR*, abs/2502.00816, 2025.

- [32] Abdul Fatir Ansari, Lorenzo Stella, Ali Caner Türkmen, Xiyuan Zhang, Pedro Mercado, Huibin Shen, Oleksandr Shchur, Syama Sundar Rangapuram, Sebastian Pineda-Arango, Shubham Kapoor, Jasper Zschiegner, Danielle C. Maddix, Michael W. Mahoney, Kari Torkkola, Andrew Gordon Wilson, Michael Bohlke-Schneider, and Yuyang Wang. Chronos: Learning the language of time series. *CoRR*, abs/2403.07815, 2024.
- [33] Nan Huang, Haishuai Wang, Zihuai He, Marinka Zitnik, and Xiang Zhang. Repurposing foundation model for generalizable medical time series classification. *CoRR*, abs/2410.03794, 2024.
- [34] Michael Wornow, Yizhe Xu, Rahul Thapa, Birju S. Patel, Ethan Steinberg, Scott L. Fleming, Michael A. Pfeffer, Jason Alan Fries, and Nigam H. Shah. The shaky foundations of large language models and foundation models for electronic health records. *npj Digit. Medicine*, 6, 2023.
- [35] Lin Lawrence Guo, Jason Alan Fries, Ethan Steinberg, Scott Lanyon Fleming, Keith E. Morse, Catherine Aftandilian, José D. Posada, Nigam Shah, and Lillian Sung. A multi-center study on the adaptability of a shared foundation model for electronic health records. *npj Digit. Medicine*, 7(1), 2024.
- [36] Rahul Thapa, Bryan He, Magnus Ruud Kjær, Hyatt E. Moore IV, Gauri Ganjoo, Emmanuel Mignot, and James Zou. Sleepfm: Multi-modal representation learning for sleep across brain activity, ECG and respiratory signals. In *ICML*. OpenReview.net, 2024.
- [37] Boris N. Oreshkin, Dmitri Carпов, Nicolas Chapados, and Yoshua Bengio. N-BEATS: neural basis expansion analysis for interpretable time series forecasting. In *ICLR*. OpenReview.net, 2020.
- [38] Jianlin Su, Murtadha H. M. Ahmed, Yu Lu, Shengfeng Pan, Wen Bo, and Yunfeng Liu. Roformer: Enhanced transformer with rotary position embedding. *Neurocomputing*, 568: 127063, 2024.
- [39] Ricky T. Q. Chen, Yulia Rubanova, Jesse Bettencourt, and David Duvenaud. Neural ordinary differential equations. In *Advances in Neural Information Processing Systems (NeurIPS)*, volume 31, 2018. URL <https://arxiv.org/abs/1806.07366>.
- [40] Harry Rubin-Falcone, Joyce M. Lee, and Jenna Wiens. Forecasting with sparse but informative variables: A case study in predicting blood glucose. In *AAAI*, pages 9650–9657. AAAI Press, 2023.
- [41] Hao Li, Yu-Hao Huang, Chang Xu, Viktor Schlegel, Ren-He Jiang, Riza Batista-Navarro, Goran Nenadic, and Jiang Bian. Bridge: Bootstrapping text to control time-series generation via multi-agent iterative optimization and diffusion modelling. *arXiv preprint arXiv:2503.02445*, 2025.
- [42] Renhe Jiang, Zhaonan Wang, Yudong Tao, Chuang Yang, Xuan Song, Ryosuke Shibasaki, Shu-Ching Chen, and Mei-Ling Shyu. Learning social meta-knowledge for nowcasting human mobility in disaster. In *WWW*, pages 2655–2665. ACM, 2023.
- [43] Qingxiong Tan, Mang Ye, Grace Lai-Hung Wong, and Pong Chi Yuen. Cooperative joint attentive network for patient outcome prediction on irregular multi-rate multivariate health data. In *IJCAI*, pages 1586–1592. ijcai.org, 2021.
- [44] Yuchao Qin, Mihaela van der Schaar, and Changhee Lee. T-phenotype: Discovering phenotypes of predictive temporal patterns in disease progression. In *AISTATS*, volume 206 of *Proceedings of Machine Learning Research*, pages 3466–3492. PMLR, 2023.
- [45] Irene Y. Chen, Rahul G. Krishnan, and David A. Sontag. Clustering interval-censored time-series for disease phenotyping. In *AAAI*, pages 6211–6221. AAAI Press, 2022.
- [46] Xinlu Zhang, Shiyang Li, Zhiyu Chen, Xifeng Yan, and Linda Ruth Petzold. Improving medical predictions by irregular multimodal electronic health records modeling. In *International Conference on Machine Learning*, pages 41300–41313. PMLR, 2023.

- [47] Dingwen Li, Bing Xue, Christopher Ryan King, Bradley A. Fritz, Michael Avidan, Joanna Abraham, and Chenyang Lu. Self-explaining hierarchical model for intraoperative time series. In *ICDM*, pages 1041–1046. IEEE, 2022.
- [48] Xi Yang, Yuan Zhang, and Min Chi. Multi-series time-aware sequence partitioning for disease progression modeling. In *IJCAI*, pages 3581–3587. ijcai.org, 2021.
- [49] Thi Kieu Khanh Ho and Narges Armanfard. Self-supervised learning for anomalous channel detection in EEG graphs: Application to seizure analysis. In *AAAI*, pages 7866–7874. AAAI Press, 2023.
- [50] Shuai Zhang, Jianxin Li, Haoyi Zhou, Qishan Zhu, Shanghang Zhang, and Danding Wang. MERITS: medication recommendation for chronic disease with irregular time-series. In *ICDM*, pages 1481–1486. IEEE, 2021.
- [51] Hangting Ye, Zhining Liu, Wei Cao, Amir M. Amiri, Jiang Bian, Yi Chang, Jon D. Lurie, Jim Weinstein, and Tie-Yan Liu. Web-based long-term spine treatment outcome forecasting. In *KDD*, pages 3082–3092. ACM, 2023.
- [52] Defu Cao, James Enouen, Yujing Wang, Xiangchen Song, Chuizheng Meng, Hao Niu, and Yan Liu. Estimating treatment effects from irregular time series observations with hidden confounders. In *AAAI*, pages 6897–6905. AAAI Press, 2023.
- [53] David J. McIver and John S. Brownstein. Wikipedia usage estimates prevalence of influenza-like illness in the united states in near real-time. *PLoS Comput. Biol.*, 10(4), 2014.
- [54] Manuel Burger, Fedor Sergeev, Malte Londschien, Daphné Chopard, Hugo Yèche, Eike Gerdes, Polina Leshetkina, Alexander Morgenroth, Zeynep Babür, Jasmina Bogojeska, et al. Towards foundation models for critical care time series. *arXiv preprint arXiv:2411.16346*, 2024.
- [55] Shruti Kaushik, Abhinav Choudhury, Pankaj Kumar Sheron, Nataraj Dasgupta, Sayee Natarajan, Larry A. Pickett, and Varun Dutt. AI in healthcare: Time-series forecasting using statistical, neural, and ensemble architectures. *Frontiers Big Data*, 3:4, 2020.
- [56] Ming Jin, Shiyu Wang, Lintao Ma, Zhixuan Chu, James Y Zhang, Xiaoming Shi, Pin-Yu Chen, Yuxuan Liang, Yuan-Fang Li, Shirui Pan, et al. Time-llm: Time series forecasting by reprogramming large language models. *arXiv preprint arXiv:2310.01728*, 2023.
- [57] Nate Gruver, Marc Finzi, Shikai Qiu, and Andrew G Wilson. Large language models are zero-shot time series forecasters. *Advances in Neural Information Processing Systems*, 36:19622–19635, 2023.
- [58] Xu Liu, Junfeng Hu, Yuan Li, Shizhe Diao, Yuxuan Liang, Bryan Hooi, and Roger Zimmermann. Unitime: A language-empowered unified model for cross-domain time series forecasting. In *Proceedings of the ACM Web Conference 2024*, pages 4095–4106, 2024.
- [59] Yuqi Nie, Nam H Nguyen, Phanwadee Sinthong, and Jayant Kalagnanam. A time series is worth 64 words: Long-term forecasting with transformers. *arXiv preprint arXiv:2211.14730*, 2022.
- [60] Yong Liu, Guo Qin, Xiangdong Huang, Jianmin Wang, and Mingsheng Long. Autotimes: Autoregressive time series forecasters via large language models. *Advances in Neural Information Processing Systems*, 37:122154–122184, 2024.
- [61] Colin Raffel, Noam Shazeer, Adam Roberts, Katherine Lee, Sharan Narang, Michael Matena, Yanqi Zhou, Wei Li, and Peter J. Liu. Exploring the limits of transfer learning with a unified text-to-text transformer. *J. Mach. Learn. Res.*, 21:140:1–140:67, 2020.
- [62] Patrick Kidger. On neural differential equations. *arXiv preprint arXiv:2202.02435*, 2022.
- [63] Albert Gu, Karan Goel, and Christopher Ré. Efficiently modeling long sequences with structured state spaces. *arXiv preprint arXiv:2111.00396*, 2021.
- [64] Jimmy TH Smith, Andrew Warrington, and Scott W Linderman. Simplified state space layers for sequence modeling. *arXiv preprint arXiv:2208.04933*, 2022.

- [65] Yulia Rubanova, Ricky T. Q. Chen, and David Duvenaud. Latent odes for irregularly-sampled time series. *CoRR*, abs/1907.03907, 2019.
- [66] Chenxi Sun, Shenda Hong, Moxian Song, and Hongyan Li. A review of deep learning methods for irregularly sampled medical time series data. *arXiv preprint arXiv:2010.12493*, 2020.
- [67] Mona Schirmer, Mazin Eltayeb, Stefan Lessmann, and Maja Rudolph. Modeling irregular time series with continuous recurrent units. In *International conference on machine learning*, pages 19388–19405. PMLR, 2022.
- [68] Yu Ma, Zhining Liu, Chenyi Zhuang, Yize Tan, Yi Dong, Wenliang Zhong, and Jinjie Gu. Non-stationary time-aware kernelized attention for temporal event prediction. In *Proceedings of the 28th ACM SIGKDD conference on knowledge discovery and data mining*, pages 1224–1232, 2022.
- [69] Da Xu, Chuanwei Ruan, Evren Korpeoglu, Sushant Kumar, and Kannan Achan. Self-attention with functional time representation learning. *Advances in neural information processing systems*, 32, 2019.
- [70] Yuan Zhang. Attain: Attention-based time-aware lstm networks for disease progression modeling. In *In Proceedings of the 28th International Joint Conference on Artificial Intelligence (IJCAI-2019)*, pp. 4369-4375, Macao, China., 2019.
- [71] Aakanksha Chowdhery, Sharan Narang, Jacob Devlin, Maarten Bosma, Gaurav Mishra, Adam Roberts, Paul Barham, Hyung Won Chung, Charles Sutton, Sebastian Gehrmann, Parker Schuh, Kensen Shi, Sasha Tsvyashchenko, Joshua Maynez, Abhishek Rao, Parker Barnes, Yi Tay, Noam Shazeer, Vinodkumar Prabhakaran, Emily Reif, Nan Du, Ben Hutchinson, Reiner Pope, James Bradbury, Jacob Austin, Michael Isard, Guy Gur-Ari, Pengcheng Yin, Toju Duke, Anselm Levskaya, Sanjay Ghemawat, Sunipa Dev, Henryk Michalewski, Xavier Garcia, Vedant Misra, Kevin Robinson, Liam Fedus, Denny Zhou, Daphne Ippolito, David Luan, Hyeontaek Lim, Barret Zoph, Alexander Spiridonov, Ryan Sepassi, David Dohan, Shivani Agrawal, Mark Omernick, Andrew M. Dai, Thanumalayan Sankaranarayanan Pillai, Marie Pellat, Aitor Lewkowycz, Erica Moreira, Rewon Child, Oleksandr Polozov, Katherine Lee, Zongwei Zhou, Xuezhi Wang, Brennan Saeta, Mark Diaz, Orhan Firat, Michele Catasta, Jason Wei, Kathy Meier-Hellstern, Douglas Eck, Jeff Dean, Slav Petrov, and Noah Fiedel. Palm: Scaling language modeling with pathways. *J. Mach. Learn. Res.*, 24:240:1–240:113, 2023.
- [72] Alistair EW Johnson, Tom J Pollard, Lu Shen, Li-wei H Lehman, Mengling Feng, Mohammad Ghassemi, Benjamin Moody, Peter Szolovits, Leo Anthony Celi, and Roger G Mark. Mimic-iii, a freely accessible critical care database. *Scientific data*, 3(1):1–9, 2016.
- [73] Alistair Johnson, Lucas Bulgarelli, Tom Pollard, Steven Horng, Leo Anthony Celi, and Roger Mark. Mimic-iv. *PhysioNet*. Available online at: <https://physionet.org/content/mimiciv/1.0/>(accessed August 23, 2021), pages 49–55, 2020.
- [74] Patrick Wagner, Nils Strodthoff, Ralf-Dieter Boussejot, Dieter Kreiseler, Fatima I Lunze, Wojciech Samek, and Tobias Schaeffter. Ptb-xl, a large publicly available electrocardiography dataset. *Scientific data*, 7(1):1–15, 2020.
- [75] Bob Kemp, Aeilko H Zwinderman, Bert Tuk, Hilbert AC Kamphuisen, and Josefiën JL Obery. Analysis of a sleep-dependent neuronal feedback loop: the slow-wave microcontinuity of the eeg. *IEEE Transactions on Biomedical Engineering*, 47(9):1185–1194, 2000.
- [76] Daniel R Miller, Gurpreet S Dhillon, Nicholas Bambos, Andrew Y Shin, and David Scheinker. Waves—the lucile packard children’s hospital pediatric physiological waveforms dataset. *Scientific Data*, 10(1):124, 2023.
- [77] Ikaro Silva, George Moody, Daniel J Scott, Leo A Celi, and Roger G Mark. Predicting in-hospital mortality of icu patients: The physionet/computing in cardiology challenge 2012. In *2012 computing in cardiology*, pages 245–248. IEEE, 2012.

- [78] Matthew A Reyna, Christopher S Josef, Russell Jeter, Supreeth P Shashikumar, M Brandon Westover, Shamim Nemati, Gari D Clifford, and Ashish Sharma. Early prediction of sepsis from clinical data: the physionet/computing in cardiology challenge 2019. *Critical care medicine*, 48(2):210–217, 2020.
- [79] George B Moody and Roger G Mark. The impact of the mit-bih arrhythmia database. *IEEE engineering in medicine and biology magazine*, 20(3):45–50, 2001.
- [80] Ensheng Dong, Jeremy Ratcliff, Tamara D Goyea, Aaron Katz, Ryan Lau, Timothy K Ng, Beatrice Garcia, Evan Bolt, Sarah Prata, David Zhang, et al. The johns hopkins university center for systems science and engineering covid-19 dashboard: data collection process, challenges faced, and lessons learned. *The lancet infectious diseases*, 22(12):e370–e376, 2022.
- [81] Chang Wei Tan, Christoph Bergmeir, Francois Petitjean, and Geoffrey I Webb. Monash university, uea, ucr time series extrinsic regression archive. *arXiv preprint arXiv:2006.10996*, 2020.
- [82] Haixu Wu, Tengge Hu, Yong Liu, Hang Zhou, Jianmin Wang, and Mingsheng Long. Timesnet: Temporal 2d-variation modeling for general time series analysis. In *ICLR*. OpenReview.net, 2023.
- [83] Mononito Goswami, Konrad Szafer, Arjun Choudhry, Yifu Cai, Shuo Li, and Artur Dubrawski. MOMENT: A family of open time-series foundation models. In *ICML*. OpenReview.net, 2024.
- [84] Azul Garza and Max Mergenthaler Canseco. Timegpt-1. *CoRR*, abs/2310.03589, 2023.
- [85] Yong Liu, Haoran Zhang, Chenyu Li, Xiangdong Huang, Jianmin Wang, and Mingsheng Long. Timer: Generative pre-trained transformers are large time series models. In *ICML*. OpenReview.net, 2024.
- [86] Kashif Rasul, Arjun Ashok, Andrew Robert Williams, Hena Ghonia, Rishika Bhagwatkar, Arian Khorasani, Mohammad Javad Darvishi Bayazi, George Adamopoulos, Roland Riachi, Nadhir Hassen, et al. Lag-Llama: Towards foundation models for probabilistic time series forecasting. *arXiv preprint arXiv:2310.08278*, 2023.
- [87] Weijia Zhang, Chenlong Yin, Hao Liu, Xiaofang Zhou, and Hui Xiong. Irregular multivariate time series forecasting: A transformable patching graph neural networks approach. In *ICML*. OpenReview.net, 2024.
- [88] Yulia Rubanova, Tian Qi Chen, and David Duvenaud. Latent ordinary differential equations for irregularly-sampled time series. In *NeurIPS*, pages 5321–5331, 2019.

A Further Related Work

In this section, we delve deeper into the related work on (medical) time series foundation models. Current research efforts in universal forecasting with time series foundation models can be broadly classified into four categories, as summarized in Table 6:

(i) **Encoder-only models.** Moirai is trained on the LOTSA dataset comprising 27B time points, with model sizes up to 311M parameters [27]. MOMENT, based on the T5 architecture, is pretrained on the Time-series Pile dataset containing approximately 1B time points, reaching up to 385M parameters [83].

(ii) **Encoder-decoder models,** exemplified by Chronos [32], which tokenizes time series data via scaling and quantization, training on both public and synthetic datasets, offers pre-trained models at multiple scales, with the largest containing up to 710M parameters.

(iii) **Decoder-only models.** TimesFM is trained on a corpus of 100B time points, with model sizes up to 500M parameters [29]. Lag-Llama focuses on univariate probabilistic forecasting, utilizing a decoder-only Transformer architecture with up to 200M parameters [86]. Timer is a generative pre-trained Transformer model designed for large-scale time series modeling, with a base version containing 84M parameters and pre-trained on 260B time points [85].

(iv) **Mixture-of-Experts architectures.** Recent models adopt sparse Mixture-of-Experts (MoE) architectures to enhance scalability and efficiency. Time-MoE [28] scales to 2.4B parameters with only a few experts activated per input, while Moirai-MoE [30] achieves token-level specialization without frequency heuristics, improving adaptability and inference cost.

Table 6: Comparison between time series models.

Method	MIRA (Ours)	Sundial (2025)	Time-MoE (2024)	Moirai-MoE (2024)	Moirai (2024)	TimesFM (2024)	Moment (2024)	Chronos (2024)	Timer (2024)	Lag-Llama (2023)	TimeGPT (2023)
Architecture	Decoder	Decoder	Decoder	Decoder	Encoder	Decoder	Encoder	EncDec	Decoder	Decoder	EncDec
(Max) Model Size	455M	444M	2.4B	1.1B	311M	500M	385M	710M	67M	200M	Unknown
Input Token	Point	Patch	Point	Patch	Patch	Patch	Patch	Point	Patch	Point	Patch
Dataset Scale	454B	1TB	309B	27B	27B/231B*	100B	1.13B	84B	29B	0.36B	100B
Max Length	512	2880	4096	5000	5000	512	512	512	1440	1024	Unknown
FFN	Sparse	Dense	Sparse	Sparse	Dense	Dense	Dense	Dense	Dense	Dense	Dense

* Depend on the way of calculation according to the original paper.

B Time Quantization Procedure

To ensure numerical stability and strictly increasing temporal inputs, we adopt a robust quantization strategy for irregular timestamps. The goal is to discretize time points with a suitable resolution while guaranteeing uniqueness. This is particularly important when encoding timestamps for attention-based models, where duplicate or non-monotonic inputs can lead to numerical or semantic inconsistencies.

The procedure begins with a predefined initial resolution (e.g., 1.0) and iteratively reduces it by a shrink factor (e.g., 10) until all quantized time points become unique. In each iteration, the algorithm rounds the original timestamps to the current resolution and checks for duplicates. If uniqueness is achieved, the quantized sequence is returned.

If, after a fixed number of iterations, uniqueness cannot be guaranteed, a fallback mechanism is triggered. In this case, small additive jitter is applied to break ties while preserving temporal ordering. The jitter is dynamically determined based on the magnitude of the input values, ensuring that the perturbation is both numerically safe and practically negligible.

Finally, the adjusted timestamps are cast to 32-bit floating-point precision and verified again for uniqueness. If rare collisions still exist due to floating-point rounding, a second corrective jitter step is applied.

This method ensures that all quantized timestamps are:

- **Strictly increasing**, preserving temporal semantics;
- **Resolution-adaptive**, automatically selecting the finest possible scale without manual tuning;
- **Numerically stable**, avoiding floating-point collisions and degenerate attention behavior.

C Mathematical Analysis of CT-RoPE

C.1 Theoretical Properties

Linear Angle Scaling For any timestamp $t \geq 0$, the rotation angles grow linearly with time:

$$\theta_i(t) = \omega_i \cdot t \quad (13)$$

where $\omega_i = 10000^{-2i/d}$ are fixed angular frequencies.

Proof. Direct from Equation (1) in the main text. The linear formulation preserves temporal causality while maintaining bounded rotation magnitudes through exponentially decaying frequencies:

$$\omega_i = \exp\left(-\frac{2i}{d} \ln 10000\right) \quad (14)$$

This ensures higher dimensions receive progressively smaller rotations.

Relative Position Encoding The inner product between rotated vectors depends only on the temporal difference:

$$\langle R_{\Theta, t_i} q, R_{\Theta, t_j} k \rangle = \langle q, R_{\Theta, |t_i - t_j|} k \rangle \quad (15)$$

Proof. Using rotation matrix properties:

$$R_{\Theta, t_i}^\top R_{\Theta, t_j} = \prod_{k=0}^{d/2-1} \begin{bmatrix} \cos(\omega_k(t_j - t_i)) & \sin(\omega_k(t_j - t_i)) \\ -\sin(\omega_k(t_j - t_i)) & \cos(\omega_k(t_j - t_i)) \end{bmatrix} \quad (16)$$

$$= R_{\Theta, t_j - t_i} = R_{\Theta, |t_i - t_j|} \quad (17)$$

The absolute difference emerges from $\cos(-\theta) = \cos(\theta)$ and $\sin(-\theta) = -\sin(\theta)$.

C.2 Rotation Matrix Construction

For a d -dimensional model (even dimension), define block-diagonal rotation matrix:

$$R_{\Theta, t} = \bigoplus_{i=0}^{d/2-1} \begin{bmatrix} \cos(\omega_i t) & -\sin(\omega_i t) \\ \sin(\omega_i t) & \cos(\omega_i t) \end{bmatrix} \quad (18)$$

with key properties:

- **Norm Preservation:** $\|R_{\Theta, t} x\| = \|x\|, \forall x \in \mathbb{R}^d$
- **Temporal Ordering:** $t_1 < t_2 \Rightarrow \theta_i(t_1) < \theta_i(t_2)$
- **Differentiable:** $\frac{\partial R_{\Theta, t}}{\partial t}$ exists $\forall t > 0$

C.3 Attention Mechanism Extension

The scaled dot-product attention becomes:

$$\text{Attention}(Q, K, V) = \text{softmax} \left(\frac{(R_{\Theta, t_Q} Q)(R_{\Theta, t_K} K)^\top}{\sqrt{d}} \right) V \quad (19)$$

where t_Q and t_K are query/key timestamps respectively. This maintains:

- **Temporal Locality:** $\lim_{\Delta t \rightarrow 0} \|R_{\Theta, t+\Delta t} - R_{\Theta, t}\| = \mathcal{O}(\Delta t)$
- **Causality:** For $t_Q > t_K$, relative rotations prevent information leakage
- **Efficiency:** Requires only $\mathcal{O}(d)$ extra computation vs standard attention

D Neural ODE

Gradient Computation via Adjoint Sensitivity For end-to-end training, gradients of a loss function \mathcal{L} (computed based on the final prediction) with respect to the ODE parameters θ_{ODE} and the initial state h_N are efficiently computed using the adjoint sensitivity method [39]. This involves solving a backward-in-time ODE for the adjoint state $a(s) = \partial \mathcal{L} / \partial h(s)$:

$$\frac{da(s)}{ds} = -a(s)^\top \frac{\partial f_{ODE}}{\partial h}(s - t_N, h(s); \theta_{ODE}) \quad (20)$$

with the terminal condition $a(t_{N+1}) = \partial \mathcal{L} / \partial h'_{N+1}$. The required gradients are then computed via integrals involving the adjoint state $a(s)$.

Algorithm 1 Neural ODE State Transition

Require: Hidden state \mathbf{h}_N , timestamps t_N, t_{N+1}

Ensure: Evolved state $\tilde{\mathbf{h}}(t_{N+1})$

- 1: Configure ODE solver tolerances: $\text{rtol} \leftarrow 10^{-6}, \text{atol} \leftarrow 10^{-6}$
 - 2: Solve ODE: $\tilde{\mathbf{h}}(t_{N+1}) \leftarrow \text{odeint}(f_{ODE}, \mathbf{h}_N, [t_N, t_{N+1}])$
 - 3: Return final state: $\tilde{\mathbf{h}}(t_{N+1})[-1]$
-

Stability Considerations To promote numerical stability and ensure the dynamics function f_{ODE} remains well-behaved (e.g., satisfies Lipschitz conditions), techniques like spectral normalization can be applied to the weights θ_{ODE} of the neural network implementing f_{ODE} . This helps control the Lipschitz constant L of f_{ODE} with respect to h , contributing to bounded error propagation during integration as characterized by bounds of the form:

$$\|h_{ODE}(t_{N+1}) - h_{\text{true}}(t_{N+1})\| \leq \mathcal{O}\left(\frac{M}{L}(e^{L(t_{N+1}-t_N)} - 1)\right) \quad (21)$$

where M relates to the local truncation error of the numerical solver.

D.1 Theoretical Guarantees

Our design satisfies the Picard-Lindelöf theorem conditions:

Theorem 1. *Let f_{ODE} be spectrally normalized with maximum singular value σ_{\max} . Then for prediction horizon $\Delta t = t_{N+1} - t_N$, the state evolution admits a unique solution satisfying:*

$$\|\tilde{\mathbf{h}}(t_{N+1}) - \tilde{\mathbf{h}}_N\| \leq \sigma_{\max} \Delta t e^{\sigma_{\max} \Delta t} \quad (22)$$

This bounded evolution property ensures numerical stability during long-horizon predictions.

E Pretraining Datasets

Table 7: The pre-training dataset of MIRA, which encompasses various sources.

Source	WAVES (2023)	MIMIC-III (2016)	MIMIC-IV (2020)	Sleep-EDF (2000)	PTB-XL (2020)	Total
# Pts.	4.8B	400B	48B	0.14B	1.3B	454B
%	1.06%	88.06%	10.57%	0.03%	0.29%	100.0%

Our pretraining corpus consists of five publicly available medical time series datasets, selected for their diversity in sampling frequency, modality coverage, and clinical relevance:

MIMIC-III [72] is a widely used publicly available database containing de-identified health records of over 40,000 patients admitted to intensive care units (ICUs) at the Beth Israel Deaconess Medical Center between 2001 and 2012. It includes multivariate time series of vital signs, laboratory test results, medication administrations, and clinical notes. The data exhibit irregular sampling patterns and substantial missingness, making them suitable for evaluating temporal robustness.

MIMIC-IV [73] is the successor to MIMIC-III, covering ICU and emergency department admissions from 2008 to 2019. It offers expanded variable coverage, improved data standardization, and higher temporal resolution. Time series are recorded with greater granularity across a broader range of hospital units, including both adult and pediatric care. Like MIMIC-III, it reflects realistic clinical irregularity but with enhanced data fidelity and scale.

PTB-XL [74] is a 12-lead ECG dataset sampled at 100 Hz, containing over 20,000 clinical recordings annotated with diagnostic statements. It enables robust modeling of waveform-based cardiovascular signals.

Sleep-EDF [75] contains overnight sleep EEG and respiration recordings annotated with sleep stages, collected under controlled conditions. The data are sampled at 100 Hz and exhibit moderate regularity with biologically driven transitions.

WAVES [76] is a pediatric waveform dataset that combines high-frequency physiological signals (ECG, PPG, respiration) from intensive care and operating room settings. It provides long continuous sequences with natural variability and noise.

F Model Configurations and Training Detail

Informed by recent scaling studies [28], we design MIRA in three model scales: $MIRA_{small}$ (73M parameters), $MIRA_{base}$ (114M), and $MIRA_{large}$ (455M), enabling flexible deployment across different hardware constraints. All models are trained on up to eight NVIDIA 80GB A100 GPUs with a micro-batch size of 128 and a maximum sequence length of 512. We pre-trained one epoch with each training step processes approximately 65,000 time points. We consider forecast horizons of 24, 32, 48, 64 for short-term and long-term evaluation. Following standard practice, we apply an auxiliary load balancing loss with weight $\alpha = 0.02$ to encourage expert utilization.

G Downstream Tasks and Datasets

Table 8: Characteristics of the WHO FluNet Dataset.

Dataset	Time Points	Missing Rate	Frequency	Irregular Sampling	Signal Type
WHO FluNet	5.27M	61.52%	Weekly		Case Counts
CINC 2012	5.28M	0%	Variable-specific	✓	ECG, Blood Pressure (ABP/NIBP), Respiration Rate, SpO ₂ , Laboratory Measurements, etc.
MIT-BIH	31.1M	0%	360 Hz		ECG
CinC 2019	39.5M	68.28%	Hourly	✓	Heart Rate, Respiration Rate, Temperature, Blood Pressure
Johns Hopkins COVID-19 Dataset	3.81M	0%	Daily		Case Counts, Death Counts
CDC-Influenza Hospitalizations Admissions	3.07M	27.1%	Weekly		Hospitalized Case Counts

CinC 2012[77] originates from the PhysioNet 2012 Challenge and contains multivariate time series from ICU patients. Each record includes asynchronously sampled clinical variables such as blood pressure, heart rate, and oxygen saturation, with irregular measurement frequencies and observation patterns. The forecasting task focuses on predicting future physiological values and deterioration risk based on past observations.

CinC 2019[78] Derived from the PhysioNet 2019 Challenge, this dataset includes time series recorded during in-hospital stays, including variables like vital signs, lab test results, and intervention indicators. The data are highly sparse and irregular, reflecting realistic clinical workflows. We focus on continuous value prediction using sliding window evaluation, emphasizing temporal robustness.

CDC-IHA⁴, published by the U.S. CDC, contains weekly aggregated hospital admission metrics related to respiratory diseases across U.S. jurisdictions. It includes counts for COVID-19, influenza, and RSV-related hospitalizations. The signals are inherently discrete and asynchronous across regions, with missing entries due to delayed or inconsistent reporting. The forecasting task involves predicting near-future hospitalization counts by location. We use below column in an weekly frequency: *Total Patients Hospitalized with COVID-19, Total Patients Hospitalized with Influenza, Total Patients Hospitalized with RSV, Total ICU Patients Hospitalized with COVID-19, Total ICU Patients Hospitalized with Influenza, Total ICU Patients Hospitalized with RSV.*

WHO FluNet⁵ These epidemiological datasets from the World Health Organization comprise country-level weekly flu case reports (FluNet).

MIT-BIH [79] This dataset provides annotated ECG waveform segments from patients with arrhythmias. The input is a regularly sampled 2-lead ECG sequence, and the forecasting task involves predicting future signal windows. We introduce synthetic missingness during evaluation to test robustness.

⁴<https://data.cdc.gov/Public-Health-Surveillance>

⁵<https://www.who.int/tools/fluNet>

JHU COVID-19 Dataset [80] This dataset aggregates daily COVID-19 cases and deaths by region. While data are reported at regular intervals, inconsistencies and reporting delays motivate the use of masked evaluation. Forecasting focuses on short-term case count prediction. We use this dataset in a daily frequency

CDC-Illness [82] The CDC outpatient illness dataset tracks ILI (influenza-like illness) and other symptoms across U.S. reporting centers. Although data are uniformly weekly, we mask 30% of time points to simulate partial surveillance dropout.

Heart Rate This dataset, sourced from the Monash Time Series Extrinsic Regression Archive [81], contains photoplethysmography (PPG) sequences paired with continuous heart rate values as targets. Each instance represents a short PPG segment with the goal of predicting the corresponding heart rate, making it a benchmark for physiological signal regression tasks.

H Baselines

Time-MoE [28]: A sparsely activated decoder-only Transformer model that incorporates a Mixture-of-Experts (MoE) architecture with token-level routing. Trained on over 300 billion real-world time points spanning nine domains, Time-MoE demonstrates strong zero-shot forecasting performance, especially in long-range and multi-resolution prediction. It uses autoregressive decoding and sliding window inference with shared expert regularization.

Moirai [27]: A universal forecasting backbone that uses patch-wise tokenization and any-variate self-attention. It is trained on the LOTSA dataset comprising 27 billion time points and supports forecasting across arbitrary time steps, variable sets, and resolutions. Moirai also employs resolution-adaptive projection layers to accommodate different patch sizes during inference.

Moirai-MoE [30]: An extension of Moirai that integrates a token-level MoE module into the decoder block. This allows for frequency-specific specialization without relying on handcrafted signal partitions. Moirai-MoE achieves improved generalization across domains with limited added compute, and supports both token-aware routing and auxiliary balancing loss.

TimesFM [29]: A decoder-only Transformer developed by Google Research, pre-trained on 100 billion real-world time points from diverse sources including IoT, finance, and weather. It features autoregressive generation with fixed-length context windows and shows strong performance in forecasting across hundreds of benchmarks.

Chronos [32]: A family of probabilistic time series foundation models that transform numerical sequences into quantized token representations. Chronos leverages discrete latent spaces and causal language modeling for forecasting and sampling. It supports both point and probabilistic prediction.

Timer [85]: A generative time series language model trained on a diverse mix of real-world and synthetic data. It uses next-token prediction and masked time-step modeling for flexible downstream adaptation. While architecture and scale details are less publicly documented, it has demonstrated competitive zero-shot accuracy on common forecasting benchmarks.

ContiFormer [18]: A continuous-time Transformer model that combines Neural ODEs with attention. It uses a NeuralODE kernel for modeling value transitions between observations and a standard self-attention block for relational reasoning. It is trained end-to-end on irregularly sampled series.

T-PatchGNN [87]: A graph-based model that converts univariate time series into a graph of overlapping time patches, using GNNs to capture local and global dependencies. It is especially effective for sparse and low-signal series and supports continuous-time node embedding.

Neural-CDE [88]: A continuous-time model based on controlled differential equations. It encodes the trajectory of observed data using a Neural CDE solver and predicts future values through learned hidden dynamics. Particularly suited for datasets with asynchronous observations.

ODE-RNN [65]: Combines standard RNN encoders with ODE solvers to update latent states over irregular intervals. It supports interpolation between time steps and improves temporal continuity compared to discrete RNNs.

Sundial [31] introduces a family of scalable time series foundation models trained on the extensive TimeBench dataset, comprising one trillion time points. Utilizing the novel TimeFlow Loss, Sundial

enables generative pretraining of Transformers without discrete tokenization, achieving state-of-the-art zero-shot performance across diverse forecasting benchmarks.

Moment [83] presents open-source Transformer-based models pre-trained on the Time-series Pile, a large and diverse collection of public time series data. Employing a masked time series prediction task, MOMENT demonstrates strong performance across forecasting, classification, and anomaly detection tasks, particularly in low-resource settings .

Lag-Llama [86] is a decoder-only Transformer model tailored for univariate probabilistic forecasting. By incorporating lagged inputs as covariates and pretraining on a diverse corpus of time series data, Lag-Llama exhibits robust zero-shot generalization and state-of-the-art performance upon fine-tuning on unseen datasets .

TimeGPT [84] is introduced as the first foundation model for time series analysis, capable of generating accurate predictions across diverse datasets without additional training. Leveraging advancements in deep learning, TimeGPT’s zero-shot inference outperforms traditional statistical, machine learning, and deep learning methods in both performance and efficiency .

I Evaluation Metrics

We evaluate forecasting performance using two widely adopted metrics: Mean Absolute Error (MAE) and Root Mean Squared Error (RMSE). Both are computed over all predicted time steps and variables, averaged across evaluation windows.

Mean Absolute Error (MAE) quantifies the average absolute deviation between predictions \hat{x}_t and ground truth x_t :

$$\text{MAE} = \frac{1}{N} \sum_{t=1}^N |x_t - \hat{x}_t|, \tag{23}$$

where N denotes the number of valid (unmasked) prediction points. MAE is robust to outliers and provides a direct measure of average deviation.

Root Mean Squared Error (RMSE) emphasizes larger errors by squaring deviations before averaging:

$$\text{RMSE} = \sqrt{\frac{1}{N} \sum_{t=1}^N (x_t - \hat{x}_t)^2}. \tag{24}$$

It is more sensitive to large prediction errors and penalizes high-variance outputs.

J Detailed Performance Analysis of Out-of-Distribution Benchmarks

We proved detail performance of different baselines and our model.

K Detailed Performance Analysis of In-Distribution Benchmarks

We proved detail performance of all the model pre-training on the medical corpus.

Table 9: Zero-shot forecasting performance on out-of-distribution datasets. Reported values are predicted by zero-shot forecasting model pre-trained on general corpora.

Models	Lag-Ilama		TimeGPT		Timer		Moment _{small}		Moment _{base}		Moment _{large}		Moirai-MoE _{small}		Moirai-MoE _{base}		
	RMSE	MAE	RMSE	MAE	RMSE	MAE	RMSE	MAE	RMSE	MAE	RMSE	MAE	RMSE	MAE	RMSE	MAE	
Heart Rate (10 ⁻¹)	24	1.643	1.385	1.668	1.463	1.899	1.769	3.231	2.035	3.218	2.025	3.204	2.019	1.443	1.137	1.636	1.321
	32	1.702	1.433	2.090	1.755	1.898	1.721	2.985	1.849	2.978	1.857	2.949	1.479	1.777	1.432	1.942	1.595
	48	1.813	1.528	2.592	2.198	1.898	1.667	2.787	1.738	2.764	1.726	2.734	1.711	2.374	1.927	2.523	2.095
	64	1.895	1.605	2.683	2.245	1.907	1.657	2.861	1.784	2.796	1.732	2.781	1.731	2.347	1.906	2.476	1.595
	Avg.	1.764	1.488	2.258	1.915	1.901	1.704	2.966	1.852	2.939	1.835	2.917	1.735	1.982	1.600	2.144	1.652
MIT-BIH	24	0.162	0.132	0.138	0.118	0.179	0.161	0.453	0.258	0.451	0.257	0.450	0.256	0.165	0.135	0.165	0.135
	32	0.185	0.148	0.175	0.141	0.219	0.184	0.407	0.216	0.405	0.214	0.402	0.211	0.185	0.152	0.185	0.151
	48	0.253	0.192	0.291	0.227	0.330	0.278	0.407	0.224	0.406	0.223	0.402	0.218	0.231	0.183	0.231	0.183
	64	0.268	0.203	0.321	0.256	0.292	0.230	0.401	0.216	0.402	0.217	0.396	0.210	0.252	0.198	0.253	0.198
	Avg.	0.217	0.169	0.231	0.185	0.255	0.213	0.417	0.229	0.416	0.228	0.413	0.224	0.208	0.167	0.208	0.167
CDC-IHA (10 ¹)	12	6.354	4.725	6.314	4.671	6.235	4.996	15.864	5.280	15.925	5.289	15.765	5.227	6.943	5.591	8.613	6.640
	18	5.193	3.968	5.208	3.989	4.908	3.727	12.884	4.435	12.941	4.404	12.894	4.416	5.751	4.600	5.868	4.731
	24	7.643	5.528	7.886	5.535	7.670	5.601	22.026	5.921	21.651	5.934	21.735	5.887	7.852	5.715	8.167	6.077
	30	6.935	5.162	7.206	5.245	6.881	5.104	20.436	5.593	20.008	5.524	20.363	5.511	7.852	5.715	7.906	6.001
	Avg.	6.531	4.846	6.654	4.860	6.424	4.857	17.803	5.307	17.631	5.288	17.689	5.260	7.099	5.405	7.639	5.862
JH COVID-19 (10 ²)	7	2.115	0.825	0.160	0.156	3.141	3.141	2.667	0.404	2.662	0.403	2.672	0.404	0.467	0.356	0.487	0.357
	14	3.052	1.214	0.990	0.817	2.268	2.135	3.795	0.642	3.826	0.644	3.811	0.641	0.547	0.396	0.522	0.389
	28	3.874	1.588	1.279	0.892	2.415	2.118	4.096	0.786	4.143	0.795	4.048	0.779	0.924	0.661	0.916	0.674
	90	5.342	2.101	5.087	4.459	2.765	1.917	1.749	0.378	1.756	0.377	1.724	0.373	3.871	1.486	75.64	11.34
	Avg.	3.596	1.432	1.879	1.580	2.647	2.328	3.077	0.553	3.097	0.554	3.064	0.549	1.452	0.725	19.391	3.190
ILI	24	1.385	0.989	0.904	0.507	1.246	1.174	1.548	0.989	1.545	0.992	1.547	0.989	1.634	1.385	1.583	1.349
	36	1.702	1.321	2.729	1.582	2.316	1.751	1.467	0.988	1.466	0.986	1.464	0.983	1.995	1.667	2.033	1.701
	48	1.914	1.493	2.337	1.227	2.051	1.549	1.669	1.134	1.663	1.128	1.662	1.128	2.158	1.801	2.119	1.765
	60	2.118	1.659	2.075	0.991	1.914	1.493	1.594	1.111	1.590	1.110	1.589	1.106	2.218	1.859	2.195	1.842
	Avg.	1.780	1.366	2.011	1.077	1.882	1.492	1.570	1.056	1.566	1.054	1.566	1.052	2.001	1.678	1.983	1.664

Table 10: Zero-shot forecasting performance on out-of-distribution datasets continued from last table. Reported values are predicted by zero-shot forecasting model pre-trained on general corpora.

Models	Moirai _{small}		Moirai _{base}		Moirai _{large}		Time-MoE _{base}		Time-MoE _{large}		Chronos _{small}		Chronos _{base}		Chronos _{large}		TimesFM		
	RMSE	MAE	RMSE	MAE	RMSE	MAE	RMSE	MAE	RMSE	MAE	RMSE	MAE	RMSE	MAE	RMSE	MAE	RMSE	MAE	
Heart Rate (10 ⁻¹)	24	2.326	1.921	2.208	1.773	2.032	1.597	0.450	0.364	0.602	0.469	1.283	0.521	1.131	0.444	1.185	0.484	1.621	0.730
	32	2.358	1.967	2.189	1.771	2.070	1.597	0.477	0.383	0.677	0.527	1.391	0.642	1.241	0.536	1.243	0.539	1.712	0.813
	48	2.332	1.955	2.117	1.759	2.145	1.691	0.505	0.401	0.950	0.724	1.535	0.703	1.353	0.583	1.391	0.602	1.894	0.921
	64	2.419	2.015	2.109	1.764	2.145	1.691	0.333	0.270	1.103	0.837	1.196	0.484	1.001	0.394	1.024	0.398	1.784	0.853
	Avg.	2.359	1.965	2.156	1.767	2.098	1.644	0.850	0.650	0.833	0.639	1.357	0.587	1.189	0.489	1.218	0.506	1.753	0.832
MIT-BIH	24	0.286	0.217	0.307	0.235	0.492	0.148	0.140	0.115	0.139	0.114	0.325	0.127	0.333	0.128	0.334	0.128	0.314	0.123
	32	0.311	0.231	0.336	0.253	0.443	0.111	0.188	0.146	0.191	0.149	0.390	0.169	0.407	0.171	0.392	0.167	0.375	0.155
	48	0.372	0.264	0.457	0.329	0.715	0.146	0.205	0.155	0.205	0.155	0.367	0.162	0.368	0.167	0.352	0.162	0.347	0.158
	64	0.401	0.282	0.579	0.392	0.719	0.191	0.152	0.121	0.152	0.122	0.323	0.128	0.331	0.131	0.317	0.131	0.305	0.126
	Avg.	0.343	0.249	0.421	0.302	0.593	0.149	0.171	0.135	0.172	0.135	0.353	0.147	0.361	0.149	0.350	0.147	0.335	0.141
CDC-IHA (10 ¹)	12	6.259	5.014	6.734	5.321	6.391	5.221	5.711	4.446	5.703	4.453	13.733	4.183	13.637	4.207	13.686	4.183	13.826	4.221
	18	5.761	4.589	6.277	4.877	5.856	4.731	4.986	3.854	4.964	3.787	10.711	3.407	11.099	3.581	11.693	3.832	10.666	3.487
	24	7.939	5.783	8.201	6.102	7.759	5.807	7.707	5.636	7.711	5.624	19.293	5.366	19.341	5.219	19.402	5.289	19.737	5.121
	30	7.381	5.698	8.099	5.802	7.144	5.448	6.839	5.056	6.871	4.996	18.273	4.729	19.223	4.745	19.163	4.766	18.302	4.804
	Avg.	6.835	5.271	7.328	5.526	6.788	5.302	6.311	4.748	6.312	4.715	15.502	4.421	15.825	4.438	15.986	4.517	15.633	4.408
JH COVID-19 (10 ²)	7	0.548	0.392	0.416	0.327	0.451	0.334	0.412	0.321	0.346	0.281	2.834	0.341	2.038	0.257	2.113	0.254	1.903	0.221
	14	0.998	0.694	0.522	0.388	0.484	0.365	0.654	0.434	0.421	0.331	3.626	0.570	3.058	0.375	2.993	0.361	2.653	0.305
	28	3.157	0.717	0.984	0.702	0.760	0.551	0.621	0.438	0.651	0.426	5.336	1.164	3.842	0.564	4.063	0.585	3.181	0.411
	90	2.966	0.977	2.042	0.479	0.761	0.358	0.697	0.416	0.632	0.446	7.506	2.051	6.401	1.006	4.741	0.884	1.581	0.349
	Avg.	1.917	0.695	0.991	0.474	0.614	0.402	0.596	0.402	0.512	0.371	4.826	1.031	3.835	0.551	3.478	0.521	2.329	0.322
ILI	24	1.609	1.371	1.522	1.296	1.436	1.219	1.006	0.802	1.131	0.910	1.732	1.142	1.621	1.053	1.598	1.028	1.651	0.995
	36	2.044	1.707	1.972	1.639	1.831	1.511	1.334	0.989	1.418	1.049	2.115	1.504	1.977	1.382	1.904	1.315	2.116	1.384
	48	2.138	1.780	1.967	1.631	1.977	1.616	1.441	1.035	1.491	1.073	2.249	1.521	2.127	1.433	2.031	1.368	2.249	1.521
	60	2.189	1.827	2.023	1.676	1.989	1.648	1.373	0.978	1.425	1.027	2.121	1.431	2.034	1.362	1.927	1.298	2.121	1.431
	Avg.	1.995	1.671	1.871	1.561	1.808	1.499	1.288	0.951	1.366	1.015	2.054	1.400	1.940	1.308	1.870	1.252	2.034	1.333

Table 11: Zero-shot forecasting performance on out-of-distribution datasets. Reported values are predicted by zero-shot forecasting model pre-trained on medical corpora.

Models	Moirai _{small}		Moirai _{base}		Moirai _{large}		Time-MoE _{base}		Time-MoE _{large}		Chronos _{small}		Chronos _{base}		Chronos _{large}		
	RMSE	MAE	RMSE	MAE	RMSE	MAE	RMSE	MAE	RMSE	MAE	RMSE	MAE	RMSE	MAE	RMSE	MAE	
Heart Rate (10 ⁻¹)	24	1.555	1.254	1.385	1.082	1.203	0.956	0.753	0.616	0.682	0.562	0.933	0.451	0.872	0.402	0.815	0.381
	32	2.418	2.002	2.283	1.850	1.849	1.464	0.647	0.523	0.614	0.495	1.014	0.582	0.935	0.521	0.879	0.490
	48	2.375	1.967	2.269	1.842	1.960	1.524	0.714	0.567	0.656	0.519	1.255	0.703	1.153	0.633	1.091	0.602
	64	1.843	1.515	1.692	1.370	1.387	1.108	0.477	0.390	0.461	0.375	0.996	0.484	0.901	0.394	0.824	0.358
Avg.	2.047	1.685	1.907	1.536	1.601	1.263	0.648	0.524	0.603	0.488	1.049	0.555	0.965	0.488	0.902	0.458	
MIT-BIH	24	0.219	0.196	0.179	0.145	0.167	0.137	0.137	0.112	0.127	0.103	0.285	0.127	0.293	0.128	0.284	0.118
	32	0.251	0.209	0.261	0.203	0.247	0.196	0.173	0.133	0.166	0.128	0.350	0.159	0.367	0.161	0.352	0.147
	48	0.257	0.210	0.456	0.253	0.272	0.214	0.136	0.101	0.139	0.104	0.327	0.142	0.328	0.147	0.312	0.132
	64	0.232	0.203	0.199	0.158	0.191	0.155	0.083	0.066	0.087	0.070	0.283	0.118	0.291	0.121	0.277	0.111
Avg.	0.239	0.204	0.274	0.190	0.219	0.176	0.132	0.103	0.131	0.101	0.311	0.137	0.320	0.139	0.306	0.127	
CDC-IHA (10 ¹)	12	6.243	5.153	6.605	5.257	6.607	5.215	5.663	4.296	5.702	4.345	12.733	4.083	12.637	4.107	12.586	4.083
	18	5.656	4.639	5.754	4.553	5.426	4.262	5.054	3.864	4.987	3.749	9.711	3.307	10.099	3.481	10.693	3.732
	24	7.775	5.948	7.958	5.982	7.708	5.669	7.668	5.602	7.655	5.571	18.293	5.266	18.341	5.119	18.402	5.189
	30	7.086	5.500	7.420	5.713	7.043	5.310	6.924	5.030	6.851	5.000	17.273	4.629	18.223	4.645	18.163	4.666
Avg.	6.690	5.310	6.934	5.376	6.696	5.114	6.327	4.698	6.299	4.666	14.502	4.321	14.825	4.338	14.986	4.417	
JH COVID-19 (10 ²)	7	0.373	0.311	0.599	0.442	0.385	0.201	0.340	0.272	0.329	0.258	2.634	0.301	2.038	0.257	1.913	0.204
	14	0.531	0.415	0.537	0.437	0.719	0.277	0.477	0.354	0.425	0.334	3.426	0.470	2.958	0.315	2.893	0.301
	28	0.707	0.515	0.586	0.497	0.200	0.527	0.689	0.473	0.712	0.484	4.336	1.064	3.742	0.514	3.863	0.535
	90	0.705	0.549	0.753	0.535	1.942	0.343	0.531	0.315	0.602	0.372	6.506	1.951	5.401	0.956	4.641	0.834
Avg.	0.579	0.448	0.619	0.478	0.812	0.337	0.509	0.353	0.517	0.362	4.225	0.947	3.535	0.510	3.328	0.469	
ILI	24	1.478	1.315	1.356	1.201	2.561	0.898	0.958	0.786	0.959	0.793	1.562	0.998	1.508	0.929	1.507	0.929
	36	1.581	1.327	1.457	1.204	1.546	1.465	1.221	0.939	1.245	0.960	1.911	1.188	1.822	1.165	1.704	1.115
	48	1.556	1.279	1.474	1.186	1.049	1.345	1.318	0.993	1.333	1.006	1.692	1.200	1.654	1.166	1.531	1.068
	60	1.499	1.232	1.454	1.174	0.843	1.208	1.255	0.943	1.265	0.948	1.655	1.123	1.571	1.062	1.447	0.998
Avg.	1.528	1.289	1.435	1.191	1.501	1.229	1.188	0.915	1.201	0.927	1.705	1.127	1.639	1.081	1.547	1.028	

Table 12: Zero-shot Forecasting on out-of-distribution datasets continued from last table.

Models	MIRA _{small}		MIRA _{base}		MIRA _{large}		Contiformer		T-PatchGNN		ODE-RNN		Neural-CDE		
	RMSE	MAE	RMSE	MAE	RMSE	MAE	RMSE	MAE	RMSE	MAE	RMSE	MAE	RMSE	MAE	
Heart Rate (10 ⁻¹)	24	1.112	0.914	1.055	0.874	0.932	0.778	0.737	0.636	0.653	0.501	0.879	0.646	0.616	0.562
	32	1.144	0.964	1.089	0.965	0.941	0.815	0.784	0.637	0.613	0.492	0.943	0.677	0.651	0.584
	48	1.208	1.012	1.116	1.048	0.984	0.847	0.775	0.623	0.626	0.494	0.967	0.691	0.692	0.594
	64	1.315	1.114	1.229	0.914	1.086	0.941	0.799	0.635	0.616	0.501	0.989	0.719	0.723	0.609
Avg.	1.195	1.001	1.123	0.950	0.986	0.845	0.774	0.633	0.627	0.497	0.945	0.683	0.671	0.587	
MIT-BIH	24	0.236	0.167	0.207	0.145	0.127	0.103	0.451	0.352	0.738	0.659	0.879	0.621	0.241	0.194
	32	0.261	0.181	0.237	0.163	0.128	0.103	0.453	0.354	0.675	0.606	0.882	0.623	0.242	0.196
	48	0.322	0.214	0.290	0.193	0.104	0.087	0.454	0.355	0.717	0.649	0.884	0.625	0.243	0.197
	64	0.351	0.232	0.319	0.205	0.070	0.058	0.452	0.353	0.691	0.595	0.881	0.622	0.242	0.195
Avg.	0.293	0.198	0.263	0.176	0.107	0.088	0.453	0.354	0.705	0.627	0.882	0.623	0.242	0.196	
CDC-IHA (10 ¹)	12	5.343	4.224	5.112	4.211	4.854	3.749	5.479	4.112	12.10	10.06	9.867	8.951	7.781	6.675
	18	5.943	4.753	5.615	4.427	5.296	4.215	5.501	4.123	8.824	7.383	10.073	9.036	7.823	6.717
	24	6.143	4.710	5.931	4.459	5.630	4.315	5.535	4.137	8.388	7.005	10.116	9.089	7.943	6.774
	30	6.475	5.048	6.258	4.912	5.924	4.571	5.490	4.159	8.778	7.445	10.214	9.131	8.022	6.896
Avg.	5.976	4.684	5.729	4.502	5.426	4.212	5.51	4.133	9.522	7.974	10.068	9.052	7.892	6.766	
JH COVID-19 (10 ²)	7	0.341	0.287	0.329	0.275	0.298	0.251	0.264	0.245	0.051	0.048	0.399	0.304	0.487	0.461
	14	0.395	0.342	0.382	0.330	0.354	0.302	0.313	0.287	0.213	0.174	0.416	0.321	0.511	0.486
	28	0.432	0.381	0.418	0.365	0.388	0.337	0.341	0.304	0.585	0.443	0.432	0.343	0.577	0.529
	90	0.461	0.408	0.451	0.397	0.423	0.372	0.374	0.351	0.551	0.497	0.447	0.357	0.604	0.535
Avg.	0.407	0.355	0.395	0.342	0.366	0.315	0.323	0.297	0.350	0.291	0.424	0.331	0.545	0.503	
ILI	24	1.112	0.932	1.035	0.883	0.953	0.825	0.374	0.218	0.194	0.143	0.403	0.261	0.421	0.311
	36	1.303	1.094	1.225	1.043	1.135	0.962	0.388	0.222	0.195	0.144	0.406	0.262	0.423	0.314
	48	1.346	1.101	1.278	1.054	1.155	0.973	0.393	0.225	0.195	0.143	0.411	0.265	0.422	0.314
	60	1.415	1.182	1.333	1.117	1.209	1.012	0.407	0.231	0.195	0.143	0.418	0.268	0.426	0.317
Avg.	1.294	1.077	1.218	1.024	1.113	0.943	0.391	0.224	0.195	0.143	0.410	0.264	0.423	0.314	

Table 13: Detail Performance on zero-shot forecasting performance at in-distribution setting.

Models	MIRA _{small}		MIRA _{base}		MIRA _{large}		Moirai _{small}		Moirai _{base}		Moirai _{large}		Time-MoE _{base}		Time-MoE _{large}		Chronos _{small}		Chronos _{base}		Chronos _{large}		
	RMSE	MAE	RMSE	MAE	RMSE	MAE	RMSE	MAE	RMSE	MAE	RMSE	MAE	RMSE	MAE	RMSE	MAE	RMSE	MAE	RMSE	MAE	RMSE	MAE	
SleepEDF (10 ²)	24	0.210	0.177	0.191	0.160	0.185	0.154	0.305	0.277	0.394	0.164	0.218	0.241	0.226	0.189	0.243	0.203	0.359	0.167	0.357	0.165	0.357	0.165
	36	0.219	0.184	0.199	0.165	0.193	0.158	0.308	0.269	0.554	0.181	0.271	0.312	0.237	0.196	0.261	0.215	0.445	0.207	0.450	0.210	0.448	0.209
	48	0.232	0.191	0.211	0.172	0.204	0.166	0.302	0.259	0.509	0.169	0.348	0.393	0.245	0.202	0.257	0.212	0.456	0.214	0.464	0.217	0.464	0.218
	60	0.197	0.168	0.178	0.151	0.172	0.145	0.284	0.251	1.214	0.393	0.378	0.346	0.205	0.172	0.216	0.181	0.383	0.178	0.384	0.179	0.381	0.178
Avg.	0.215	0.180	0.195	0.162	0.189	0.156	0.301	0.264	0.668	0.227	0.304	0.323	0.228	0.191	0.244	0.203	0.411	0.192	0.414	0.193	0.413	0.193	
PTB-XL	24	0.150	0.098	0.111	0.082	0.106	0.079	0.139	0.117	0.231	0.094	0.301	0.188	0.113	0.067	0.112	0.068	0.241	0.105	0.247	0.109	0.246	0.109
	36	0.142	0.106	0.122	0.091	0.116	0.087	0.181	0.123	0.209	0.082	0.303	0.075	0.114	0.065	0.112	0.063	0.224	0.100	0.225	0.104	0.224	0.104
	48	0.153	0.114	0.132	0.099	0.126	0.095	0.192	0.131	0.361	0.104	0.70	0.131	0.121	0.064	0.121	0.063	0.226	0.102	0.226	0.104	0.223	0.104
	60	0.164	0.123	0.143	0.107	0.136	0.102	0.176	0.130	0.280	0.113	0.359	0.101	0.091	0.055	0.091	0.068	0.218	0.092	0.238	0.099	0.226	0.096
Avg.	0.147	0.110	0.127	0.095	0.121	0.091	0.177	0.125	0.270	0.098	0.416	0.099	0.110	0.063	0.109	0.066	0.228	0.100	0.234	0.104	0.229	0.103	
MIMIC-III	24	0.110	0.092	0.091	0.075	0.087	0.072	0.142	0.126	0.248	0.098	0.121	0.085	0.101	0.077	0.096	0.075	0.120	0.063	0.122	0.065	0.121	0.063
	36	0.120	0.101	0.101	0.084	0.096	0.080	0.167	0.144	0.310	0.109	0.148	0.142	0.108	0.081	0.107	0.079	0.171	0.087	0.168	0.088	0.166	0.088
	48	0.132	0.110	0.112	0.093	0.107	0.088	0.179	0.152	0.187	0.142	0.232	0.156	0.119	0.104	0.116	0.096	0.193	0.098	0.195	0.100	0.193	0.102
	60	0.143	0.119	0.123	0.102	0.117	0.097	0.162	0.143	0.278	0.307	0.187	0.167	0.093	0.061	0.091	0.059	0.127	0.066	0.131	0.069	0.123	0.068
Avg.	0.126	0.106	0.107	0.089	0.102	0.084	0.163	0.141	0.256	0.164	0.172	0.138	0.105	0.081	0.103	0.078	0.153	0.079	0.154	0.080	0.151	0.080	
MIMIC-IV	24	0.093	0.079	0.071	0.059	0.071	0.048	0.259	0.236	0.241	0.195	0.286	0.116	0.060	0.070	0.089	0.069	0.283	0.115	0.285	0.116	0.286	0.117
	36	0.105	0.089	0.090	0.065	0.082	0.056	0.272	0.229	0.283	0.275	0.353	0.165	0.104	0.082	0.103	0.079	0.366	0.171	0.355	0.165	0.353	0.164
	48	0.117	0.099	0.096	0.074	0.093	0.066	0.269	0.216	0.304	0.318	0.374	0.174	0.091	0.064	0.088	0.062	0.356	0.155	0.372	0.173	0.374	0.174
	60	0.129	0.108	0.108	0.081	0.104	0.073	0.236	0.210	0.367	0.375	0.264	0.117	0.052	0.040	0.047	0.038	0.229	0.096	0.257	0.114	0.264	0.117
Avg.	0.111	0.094	0.091	0.069	0.081	0.061	0.259	0.223	0.300	0.291	0.319	0.143	0.084	0.064	0.082	0.062	0.309	0.134	0.317	0.142	0.319	0.143	
WAVES (10 ²)	24	0.132	0.120	0.125	0.105	0.119	0.099	0.170	0.153	0.187	0.180	0.145	0.183	0.151	0.126	0.132	0.119	0.152	0.102	0.151	0.101	0.151	0.101
	36	0.155	0.129	0.137	0.112	0.130	0.107	0.184	0.161	0.192	0.174	0.169	0.149	0.156	0.129	0.143	0.118	0.191	0.125	0.193	0.126	0.192	0.125
	48	0.167	0.139	0.148	0.122	0.141	0.116	0.185	0.161	0.222	0.177	0.208	0.153	0.157	0.131	0.150	0.124	0.219	0.137	0.217	0.136	0.217	0.135
	60	0.151	0.126	0.133	0.110	0.126	0.103	0.169	0.151	0.160	0.194	0.152	0.136	0.129	0.108	0.124	0.104	0.171	0.110	0.169	0.109	0.167	0.108
Avg.	0.154	0.129	0.136	0.112	0.129	0.106	0.177	0.157	0.190	0.181	0.169	0.155	0.148	0.124	0.141	0.116	0.184	0.119	0.183	0.118	0.182	0.117	